Title
PROPAGATION CHARACTERISTICS OF A HOLLOW PLASMA WAVEGUIDE

Author
Katz, Joseph E.

Publication Date
1967-05-01

UCRL-17564

cy. 2

University of California

Ernest O. Lawrence Radiation Laboratory

PROPAGATION CHARACTERISTICS OF A HOLLOW PLASMA WAVEGUIDE

DISCLAIMER

UCRL-17564

UNIVERSITY OF CALIFORNIA

Lawrence Radiation Laboratory
Berkeley, California

AEC Contract No. W-7405-eng-48

PROPAGATION CHARACTERISTICS OF A HOLLOW PLASMA WAVEGUIDE

Joseph E. Katz

(M.S. Thesis)

May 1967

Joseph E. Katz

Lawrence Radiation Laboratory
University of California
Berkeley, California

ABSTRACT

The dispersion relation for the axial propagation of electromagnetic energy in a hollow plasma waveguide is derived. The structure considered has a cross section consisting of a central cylindrical vacuum region surrounded by a plasma shell contained within a metal outer conductor. Solutions of the dispersion relation are presented which show the variation in propagation characteristics attained by varying the plasma properties, the radial dimensions, or the external magnetic field. Losses in the plasma region and the effect of finite conductivity in the metal outer conductor are considered.

Propagation characteristics of a hollow plasma waveguide resemble those of a metal circular waveguide for large axial magnetic fields, but as the axial magnetic field is reduced, the phase characteristic of the guide changes to that of a slow wave structure. The attenuation characteristic of the hollow plasma waveguide, for waves of a TM type, may be lower by several powers of ten than that of conventional metal waveguides.

Contents

I. INTRODUCTION

Present-day radio-frequency linear particle accelerators employ metal waveguides or cavity resonators to confine the intense electromagnetic fields required. This introduces two limitations at high energies. Large amounts of rf power are required to compensate the copper losses in the walls of the metal structures, and great physical lengths are required because the maximum voltage gradient is limited to a few million volts per foot of accelerator length by high-voltage breakdown between conductors in vacuum. For example, the linear accelerator at Stanford requires 240 20-MW klystrons to produce 20-GeV electrons, with most of the supplied energy used to overcome copper losses in the two-mile accelerator waveguide.

Clearly it will be of great value to develop an accelerator structure with significantly less loss than metal waveguides or cavity resonators. A structure that is only 1/1000 as lossy as the Stanford linear accelerator waveguide will require only one 5-MW klystron to overcome wall losses in the waveguide. It will be of greater interest if the same structure can hold higher voltage gradients before breakdown in vacuum. Increasing the voltage gradient the structure may hold will reduce the length required.

It has been proposed by others to construct a guide for electromagnetic energy, using a plasma, that has considerably lower loss than the best metal conductors.[1-3] If the plasma frequency, ω_p, is higher than the applied rf frequency, ω, and if the plasma collision frequency, ν, is very much lower than the rf frequency, little rf power will be transferred to the plasma. Lichtenberg has considered a plasma waveguide

consisting of two semi-infinite plasma slabs separated by a vacuum region.[1] August has considered a cylindrical vacuum region within an infinite plasma.[2] Both have considered the case of an infinite axial magnetic field and have indicated that low-loss propagation of fast waves (phase velocity greater than the velocity of light) may be achieved by using a plasma waveguide device.

The hollow plasma waveguide, hereafter also referred to as a plasmaguide, has the cross section shown in Fig. 1. A method of confining the plasma, suggested by Woodyard, is in a Philips Ion Gauge type of discharge in a strong axial external magnetic field.[3] If a ring-shaped cathode is used, the plasma formed will be hollow, and the electromagnetic energy will be confined primarily to the central vacuum core. In the proposed plasmaguide, the cyclotron frequency, ω_c, is proportional to the axial magnetic field and will enter into the solution as an independent variable. The presence of a finite cyclotron frequency makes the plasma an anisotropic medium and greatly complicates any type of analysis except by numerical methods on a high-speed digital computer.

It may be seen from the brief discussion above that the plasmaguide designer has a large number of independent variables at his disposal to achieve a favorable design. There are at least four different frequencies and at least two major linear dimensions available. In brief, these are the plasma frequency, the collision frequency, the cyclotron frequency, the applied rf frequency, the vacuum region radius, and the outer radius of the plasma region. A computer solution of the propagation characteristics of the plasmaguide which considers all these

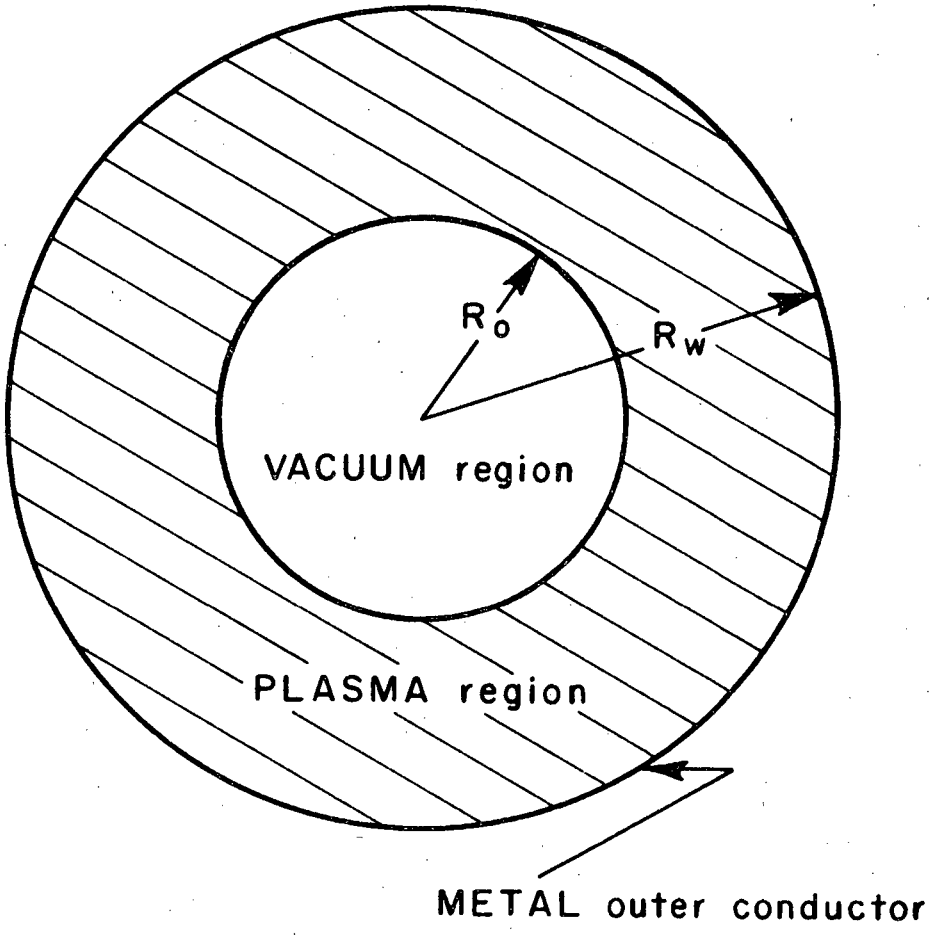

XBL675-3140

Cross section of the hollow plasma waveguide.

Fig. 1

independent variables has been developed. Several cases have been examined which show that a hollow plasma waveguide of reasonable dimensions (theoretically obtainable plasma conditions) and moderate external axial magnetic fields has powers of ten less loss than conventional metal waveguides.

The properties of the hollow plasma waveguides investigated will be described by ω-β diagrams, by plots of the axial rf electric field distribution, and by attenuation curves. No attempt will be made to analyze the behavior of the hollow plasma waveguide as a function of rf signal level. The behavior of a plasma in a strong rf field and the question of high-voltage gradients have been examined by August.[4] In the following discussion, the small-signal equivalent dielectric tensor representation of the electronic properties of the plasma region is used.

Experimental work using a plasma column to guide electromagnetic energy has been reported by Lichtenberg, Govindan, and Woodyard.[5] The Q of a partially ionized plasma with fluctuating density, created by a reflex discharge, is determined by a measurement of the decay of microwave energy in a cavity coaxial to the plasma column. The measurements indicate that the plasma Q is lower by a factor of 3 to 4 than the Q calculated from the theory. The results obtained in this discussion, for a theoretically simplified plasma, must be considered alongside the experimental difficulties and the inexplicably larger losses reported by others.[5]

II. DERIVATION OF THE FIELD EQUATIONS

1. Characterization of the Plasma

A plasma is defined here as a fully ionized gas in which the Debye length is much smaller than any other length of interest, and in which only the bulk properties of the gas are important. In addition, the plasma is assumed to be uniform everywhere (the plasma-vacuum interface is an abrupt transition).

For simplicity in calculations, the plasma is considered to be a fully ionized hydrogen gas. Partial ionization principally alters the rf losses, but not the gross electromagnetic properties of the plasma.

For use in a hollow plasma waveguide, we shall consider only low-temperature and low-density plasmas appropriate to microwave applications. If the plasma electron temperature ranges from 5 000 to 100 000°K (0.5 to 10 eV approximately), the plasma will usually be from a few per cent to 100% ionized. The densities considered will range from 10^{10} to 10^{13} (charged) particles per cm^3. For comparison, thermonuclear fusion plasmas have temperatures and densities on the order of 10^8 °K and 10^{14} particles per cm^3 and higher.

The plasma properties may be described by several characteristic frequencies. They are the following:

(a) The plasma frequency, ω_p, is the characteristic relaxation frequency of the plasma. Neglecting temperature corrections, it is given by

$$\omega_p = \left(\frac{n_e e^2}{m \epsilon_0}\right)^{1/2}, \qquad (1)$$

where n_e = electron density, electrons/m_3,

e = electronic charge, 1.602×10^{-19} coulomb,

m = electron rest mass, 9.1091×10^{-31} kg,

ϵ_0 = the permittivity of vacuum, 8.8542×10^{-12} farad/m.

(b)The cyclotron frequency, ω_c, is the frequency of rotation of electrons in a magnetic field; it is given by

$$\omega_c = (e/m)B_0, \tag{2}$$

(c) The collision frequency, ν, represents an energy loss mechanism in the plasma. For a fully ionized plasma, there are three types of collisions, electron-electron, ion-ion, and electron-ion. The first and second types do not change the total energy or momentum of the electrons or the ions, but are useful in establishing equilibrium distributions of these particles. Collisions of the third type transfer energy and momentum between the electrons and the ions, and are a mechanism for transferring energy from an electromagnetic wave to the plasma.

(d) The average electron-ion collision frequency as given by Shkarofsky[6] is

$$\nu = \left(\frac{3}{2\pi}\right)^{1/2} 8\pi n_e \left(\frac{3K_B T_e}{2m}\right)^{1/2} \left(\frac{e^2}{12\pi\epsilon_0 K_B T_e}\right)^2 \times \ln\left[\left(\frac{K_B T_e \epsilon_0}{n_e e^2}\right)^{1/2} \left(\frac{12\pi\epsilon_0 K_B T_e}{e^2}\right)\right],$$

where K_B = Boltzmann's constant and T_e = the electron temperature in ^oK.

For a hydrogen plasma

$$\nu = \frac{\ln\left[7.18\times10^{8}\, T_e^{3/2}/\omega_p\right]}{\left[8.08\times10^{8}\, T_e^{3/2}/\omega_p^{2}\right]} . \tag{3}$$

For small signals, the electronic properties of the plasma region may be specified by an equivalent dielectric tensor. A detailed description of the derivation of the equivalent dielectric tensor representation for the plasma region may be found in Spitzer.[7] For cylindrical or Cartesian coordinates we use

$$\|\epsilon_r\| = \begin{Vmatrix} \epsilon_{11} & i\epsilon_{12} & 0 \\ -i\epsilon_{12} & \epsilon_{11} & 0 \\ 0 & 0 & \epsilon_{33} \end{Vmatrix} , \tag{4}$$

where

$$\epsilon_{11} = 1 - \frac{\omega_p^2(\omega + i\nu)}{\omega\left[(\omega+i\nu)^2 - \omega_c^2\right]} ,$$

$$\epsilon_{12} = \frac{-\omega_c\omega_p^2}{\omega\left[(\omega+i\nu)^2 - \omega_c^2\right]} ,$$

$$\epsilon_{33} = 1 - \frac{\omega_p^2}{\omega(\omega+i\nu)} .$$

The rf fields are assumed to have an exp (γz - iωt) dependence. If there are any losses in the plasma region, the propagation constant, γ, will be complex. Then, $\gamma = \alpha + i\beta$ where α = the attenuation constant and β = the phase constant.

2. Plasma Region Field Equations

Many investigators have discussed metal waveguides, filled or partially filled along the center with plasma.[8,10-12] Although the geometry and operating conditions studied by these investigators differ

from the case presented here, many of their plasma region results apply here.

Maxwell's equations in the plasma region are

$$\nabla \times \vec{E} = i\omega \mu_0 \vec{H} \ ,$$

$$\nabla \times \vec{H} = -i\omega \epsilon_0 \|\epsilon_r\| \vec{E} \ ,$$

$$\nabla \cdot \vec{H} = 0 \ ,$$

$$\nabla \cdot \epsilon_0 \|\epsilon_r\| \vec{E} = 0 \ ,$$

where μ_0 = the permeability of vacuum, $4\pi \times 10^{-7}$ henry/m.

For the case of no losses, $\alpha = 0$ and $\frac{\partial}{\partial z} = i\beta$, $\frac{\partial}{\partial t} = i\omega$.

The above set of equations may be expanded in cylindrical coordinates and manipulated to give a set of four equations expressing the transverse electric and magnetic fields in terms of the axial electric and magnetic fields:

$$K1\, E_r = i\beta \left[K2 \frac{\partial E_z}{\partial r} - i k \frac{\epsilon_{12}}{r} \frac{\partial E_z}{\partial \theta} \right] + k\eta \left[\frac{iK2}{r} \frac{\partial H_z}{\partial \theta} - k^2 \epsilon_{12} \frac{\partial H_z}{\partial r} \right], \tag{5}$$

$$K1\, E_\theta = i\beta \left[\frac{K2}{r} \frac{\partial E_z}{\partial \theta} + i k^2 \epsilon_{12} \frac{\partial E_z}{\partial r} \right] - k\eta \left[iK2 \frac{\partial H_z}{\partial r} + \frac{k^2 \epsilon_{12}}{r} \frac{\partial H_z}{\partial \theta} \right], \tag{6}$$

$$K1 H_r = i\beta \left[K2 \frac{\partial H_z}{\partial r} - i k^2 \frac{\epsilon_{12}}{r} \frac{\partial H_z}{\partial \theta} \right] + \frac{k}{\eta} \left[\beta^2 \epsilon_{12} \frac{\partial E_z}{\partial r} - \frac{iK3}{r} \frac{\partial E_z}{\partial r} \right], \tag{7}$$

$$K1 H_\theta = i\beta\left[i k^2 \epsilon_{12} \frac{\partial H_z}{\partial r} + \frac{K2}{r} \frac{\partial H_z}{\partial \theta}\right] + \frac{k}{\eta}\left[i K3 \frac{\partial E_z}{\partial r} + \beta^2 \frac{\epsilon_{12}}{r} \frac{\partial E_z}{\partial r}\right], \tag{8}$$

where

$k = \omega/c$ (wave number),

c = velocity of light in a vacuum (2.997925×10^8 m/sec),

$\eta = \sqrt{\mu_o/\epsilon_o}$ (vacuum wave impedance),

$K2 = k^2 \epsilon_{11} - \beta^2$,

$K1 = K2^2 - k^4 \epsilon_{12}^2$,

$K3 = k^2 \epsilon_{11}^2 - k^2 \epsilon_{12}^2 - \beta^2 \epsilon_{11}$.

Further manipulation of Maxwell's equations yields

$$\left[\nabla_T^2 + \left(\frac{\epsilon_{11}^2 - \epsilon_{12}^2}{\epsilon_{11}}\right) k^2 - \beta^2\right] \eta H_z = -i \frac{\epsilon_{12}\epsilon_{33}}{\epsilon_{11}} k\beta E_z ,$$

$$\left[\nabla_T^2 + \epsilon_{33} k^2 - \beta^2 \frac{\epsilon_{33}}{\epsilon_{11}}\right] E_z = i \frac{\epsilon_{12}}{\epsilon_{11}} k\beta\eta H_z ,$$

where ∇_T^2 is the transverse portion of the Laplacian operator. In cylindrical coordinates it is given by $\nabla_T^2 = \frac{1}{r}\frac{\partial}{\partial r}\left(r\frac{\partial}{\partial r}\right) + \frac{1}{r^2}\frac{\partial^2}{\partial \theta^2}$. For convenience we shall make the following definitions:

$$a_1 = \frac{\epsilon_{11}^2 - \epsilon_{12}^2}{\epsilon_{11}} k^2 - \beta^2 , \tag{9}$$

$$a_2 = \epsilon_{33} k^2 - \frac{\epsilon_{33}}{\epsilon_{11}} \beta^2 , \tag{10}$$

$$b_1 = -\frac{\epsilon_{33}\epsilon_{12}}{\epsilon_{11}} k\beta , \tag{11}$$

$$b_2 = i \frac{\epsilon_{12}}{\epsilon_{11}} k\beta . \tag{12}$$

The scalar wave equations for the axial fields may now be written

$$\left[\nabla_T^2 + a_1\right]\eta H_z = b_1 E_z, \tag{13}$$

$$\left[\nabla_T^2 + a_2\right] E_z = b_2 \eta H_z. \tag{14}$$

Equations (13) and (14) are two coupled scalar wave equations relating E_z and H_z. This pair of coupled equations must be solved simultaneously. Only under certain circumstances are pure TE or TM modes possible. If either b_1 or b_2 is equal to zero, the scalar wave equations are uncoupled. This may occur if the external magnetic field is infinite or zero. The scalar wave equations are also uncoupled at the plasmaguide cutoff frequency at which β is zero.

In other research on wave propagation in gyrotropic media, the rotational nature of both the electric and magnetic fields has been included and formal equations have been obtained.[9-11] Electrons under the influence of such fields undergo transverse as well as axial oscillations. Bevc and Everhart have defined the possible modes of wave propagation as follows:[11]

A wave is predominantly <u>transverse electric</u>, TE, if in its transverse components the contribution of the longitudinal magnetic field component exceeds the contribution of the longitudinal electric field component by at least one power of ten.

A wave is predominantly <u>transverse magnetic</u>, TM, if in its transverse components the contribution of the longitudinal electric field exceeds the contribution of the longitudinal magnetic field component by at least one power of ten.

A wave is hybrid if the contributions of the longitudinal electric and magnetic field components to transverse field components are approximately the same.

A practical hollow plasma waveguide design of a linear accelerator structure will have its operating parameters selected to maintain a TM mode of energy propagation.

Following the method of Shohet, the scalar wave equations, Eqs. (13) and (14), can be uncoupled from each other, producing two fourth-order bi-quadratic wave equations,[12]

$$\left[\nabla_T^4 + \nabla_T^2(a_1 + a_2) + a_1 a_2 - b_1 b_2\right] E_z = 0, \tag{15}$$

$$\left[\nabla_T^4 + \nabla_T^2(a_1 + a_2) + a_1 a_2 - b_1 b_2\right] H_z = 0. \tag{16}$$

The fourth-order equation for the electric or magnetic field may be factored into the product of two second-order wave equations:

$$\left[\nabla_T^2 - T_1^2\right]\left[\nabla_T^2 - T_2^2\right] E_z = 0, \tag{17}$$

where $$T_{1,2}^2 = \left[-\frac{a_1 + a_2}{2} \pm \sqrt{\left(\frac{a_1 - a_2}{2}\right)^2 + b_1 b_2}\,\right].$$

Solutions of the second-order wave equations for a cylindrical geometry are well known; they are, in fact, just Bessel's equations. The result is that, in general, E_z and H_z are the linear sums of two solutions. The general form of the solution is

$$E_j = \sum_{q} \sum_{j=1}^{2} A_{jq} e^{iq\theta} Z_q(T_j r),$$

where $Z_q(T_j r)$ denotes some cylinder function (a solution of Bessel's equation).

In general, T_j^2 is complex. If T_j^2 is a real number, and $T_j^2 < 0$, the solutions can be expressed as a linear combination of Bessel functions of the first and second kinds with real arguments [$J_q(T_j r)$ and $Y_q(T_j r)$]. If T_j^2 is a real number and $T_j^2 > 0$, the solutions can be expressed as a linear combination of modified Bessel functions of the first and second kinds with real arguments, [$I_q(T_j r)$ and $K_q(T_j r)$]. If T_j^2 is complex, either the unmodified or the modified Bessel functions are appropriate, but must be evaluated with complex arguments.

At this point in the discussion, it is instructive to consider the case in which the external axial magnetic field is infinite or zero, then b_1 and b_2 equal zero. The scalar wave equations are uncoupled; with $\omega_p > \omega$, we find that $T^2 > 0$. The solutions of the scalar wave equations are a linear combination of modified Bessel functions of the first and second kinds.

Returning to the discussion of the general case, the TM mode of electromagnetic wave propagation with no circumferential variations, $q = 0$, is the only mode of interest for possible linear accelerator applications. Therefore, the solution for the axial electric field in the plasma region may be written

$$E_z = \sum_{j=1}^{2} A_j Q_0(T_j r) + B_j W_0(T_j r), \tag{18}$$

where Q_0 represents an unmodified or a modified Bessel function of the first kind, and W_0 represents an unmodified or a modified Bessel function of the second kind.

Substituting in the coupled scalar wave equation, Eq. (14), one may write the expression for the axial magnetic field,

$$H_z = \sum_{j=1}^{2} \frac{F_j}{\eta}\left[A_j Q_0(T_j r) + B_j W_0(T_j r)\right], \tag{19}$$

where $F_j = \dfrac{T_j^2 + a_2}{b_z}$.

Substituting the above expressions for the axial fields into the previously derived expressions, Eq. (5) through (8) for the transverse fields, one obtains the equations for the transverse fields in the plasma region. (See Appendix A for the transverse field equations.)

3. Vacuum Region Field Equations

The field equations in the vacuum region are easily derived by letting ω_p go to zero in the various plasma equations. Then, ϵ_{11} and ϵ_{33} go to unity and ϵ_{12} goes to zero. The scalar wave equations for the axial fields become

$$\left[\nabla_T^2 + K4\right] E_z^v = 0, \tag{20}$$

$$\left[\nabla_T^2 + K4\right] H_z^v = 0, \tag{21}$$

where $K4 = k^2 - \beta^2$.

In the vacuum region, the scalar wave equations are separable and pure TE or TM modes may exist, but in order to satisfy the boundary conditions, both TE and TM modes must be considered.

Solutions of the scalar wave equations are Bessel functions. Bessel functions of the second kind, either unmodified or modified, are not allowed as a solution, since the vacuum region includes $r = 0$. If $K4 > 0$, the solution of either scalar wave equation is the unmodified Bessel function of the first kind. If $K4 < 0$, the solution is the

modified Bessel function of the first kind. Therefore, the solutions for the axial electric and magnetic fields in the vacuum region may be written

$$E_z^V = C Q_0(T_3 r) \tag{22}$$

and

$$H_z^V = \lambda \frac{D}{\eta} Q_0(T_3 r), \tag{23}$$

where $T3 = \left[k^2 - \beta^2 \right]^{1/2}$.

The equations for transverse fields in the vacuum region are derived similarly to those for the plasma region. The transverse field equations for the vacuum region are tabulated in Appendix A.

III. DISPERSION RELATION AND METHOD OF SOLUTION

1. Determination of the Dispersion Relation

By use of the expressions for the tangential fields, a set of six linear homogeneous equations may be written to describe the boundary conditions. The boundary conditions that must be satisfied are that

(a) the tangential components of the electric and magnetic fields must be continuous across the plasma-vacuum interface,

(b) the tangential components of the electric field must vanish at the metal wall of the outer conductor (use of a good conductor is assumed).

The six boundary conditions (four on E_z, H_z, E_θ, and H_θ at $r = R_0$, and two on E_z and E_θ at $r = R_w$) result in six linear homogeneous equations. The resultant determinant, which must be set equal to zero for a nontrivial solution, is the dispersion relation for the plasmaguide; in general it is made up of complex terms arranged as shown below

$$\begin{vmatrix} a_{11} & a_{12} & a_{13} & a_{14} & a_{15} & 0 \\ a_{21} & a_{22} & a_{23} & a_{24} & 0 & a_{26} \\ a_{31} & a_{32} & a_{33} & a_{34} & 0 & a_{36} \\ a_{41} & a_{42} & a_{43} & a_{44} & a_{45} & 0 \\ a_{51} & a_{52} & a_{53} & a_{54} & 0 & 0 \\ a_{61} & a_{62} & a_{63} & a_{64} & 0 & 0 \end{vmatrix} = 0 . \qquad (24)$$

The elements of the above determinant are tabulated in Appendix B.

2. Method of Solution

The solution of the determinantal dispersion relation is cumbersome by other than numerical methods. A digital computer program was written in FORTRAN IV language to find the complex propagation constant, γ, necessary to satisfy the dispersion relation at a given rf frequency. In general, a complex γ is necessary unless there are no losses in the plasma region ($\nu = 0$); if there are not, the propagation constant is given by $\gamma = i\beta$. In the execution of the program, the frequency is varied from the TM_{01} cutoff frequency of the hollow plasma waveguide, ω_0, to an upper frequency of three times the cutoff frequency, ω_{max}. A logical flow chart of the digital computer program to find the γ necessary to satisfy the dispersion relation is shown in Fig. 2.

The independent variables used to describe the hollow plasma waveguide are read into the computer at point A of Fig. 2. They are:

R_0 = vacuum radius in meters,

R_w/R_0 = ratio of outer conductor radius to vacuum region radius,

ν/ω = ratio of collision frequency to rf frequency,

ω_p/ω_0 = ratio of plasma frequency to plasmaguide cutoff frequency, and

ω_c/ω_p = ratio of cyclotron frequency to plasma frequency.

At point B, Fig. 2, the cutoff frequency of the plasmaguide described in the input data is computed. The derivation of the plasmaguide cutoff dispersion relation and the solution of the cutoff dispersion relation are described in Chapter IV.

At point C, Fig. 2, the elements of the equivalent dielectric tensor are computed for a frequency slightly higher than the cutoff

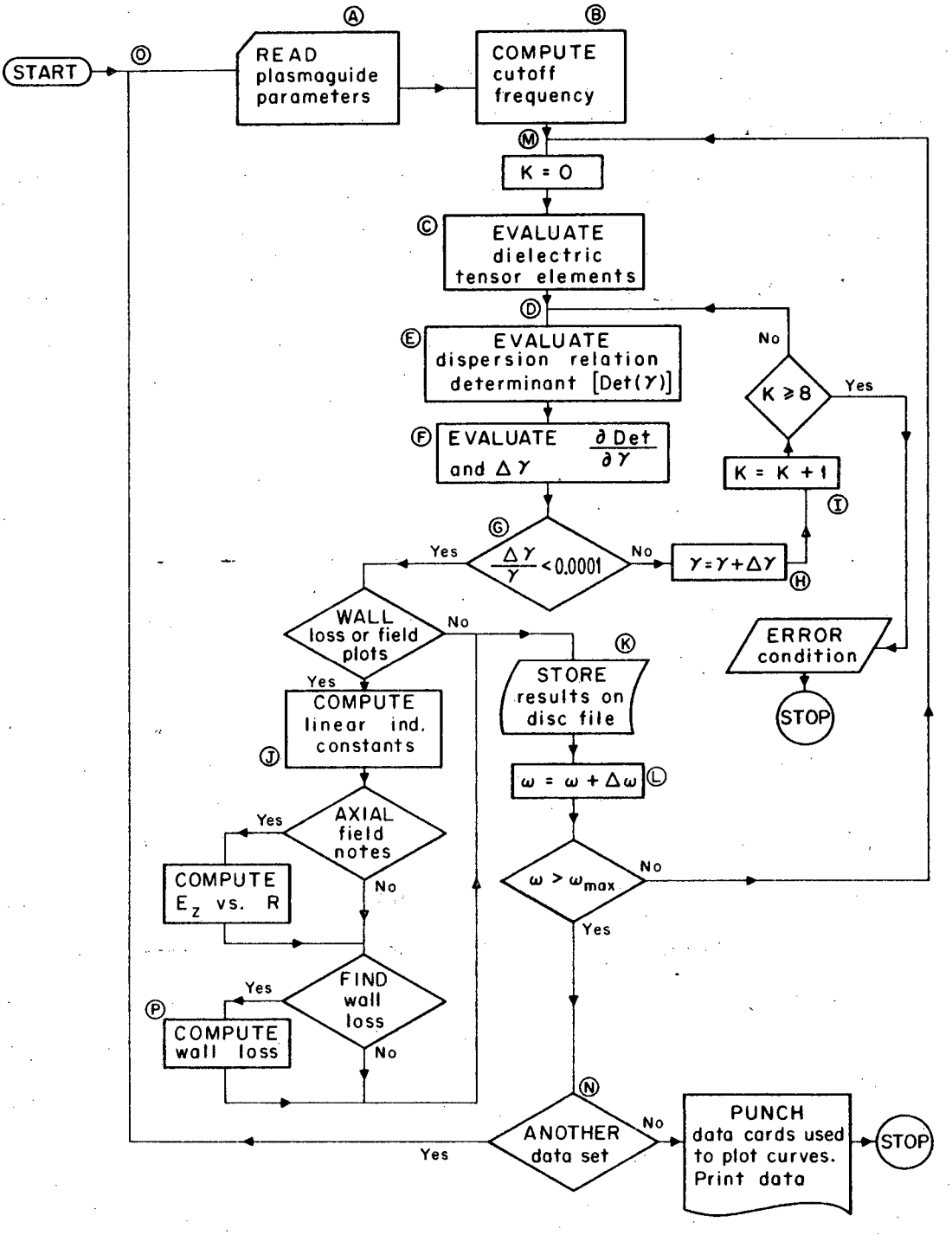

XBL675-3141

Logical flow chart of the digital computer program for the exact solution of the plasmaguide characteristics.

Fig. 2

frequency. The program is ready to search for the propagation constant necessary to satisfy the dispersion relation at this frequency. The elements of the dispersion relation determinant, as given in Appendix B, are evaluated at point D. The propagation constant of an equivalent metal guide is used as the first guess at the γ necessary to satisfy the determinantal equation. A round metal guide operating in the TM_{01} mode with the same cutoff frequency as the plasmaguide is used for comparison purposes. It is referred to as an equivalent metal guide throughout the rest of this discussion.

In determining the elements of the dispersion-relation determinant, one must evaluate unmodified and modified Bessel functions for both real and complex arguments. The computer coding to do this must be efficient and sufficiently accurate to enable one to solve for complex propagation constants when the phase constant and the attenuation constant may differ by factors as large as 10^9. To compute the desired Bessel functions, it was necessary to combine and modify several subroutines developed by other programmers.[13-15] The computed results of the Bessel function routine developed for this program were compared, for a wide range of real and complex arguments, with the National Bureau of Standards tables of Bessel functions.[16,17] The results agreed with the tables to six significant figures, the extent of the tables.

After the elements have been evaluated, the value of the determinant is computed by use of a subroutine developed for this purpose.[18] The value of the determinant, $\mathrm{Det}(\gamma)$, is in general, complex. The program then proceeds to compute the change in the assumed propagation

constant, γ, necessary to reduce the value of the determinant to zero. The procedure followed at point E, Fig. 2, is to assume one is sufficiently close to the desired γ (that satisfies the dispersion relation) to expand the function $\mathrm{Det}(\gamma)$ by means of a Taylor's series expansion about γ.[19] This method of computing the zero of a function is called the Newton-Raphson method, and is treated in many numerical analysis texts.[20,21] The result of the Taylor's series expansion, ignoring higher-order terms, is given by

$$0 = \mathrm{Det}(\gamma) + \Delta\gamma \frac{\partial \mathrm{Det}(\gamma)}{\partial \gamma} + \ldots, \tag{25}$$

where $\Delta\gamma$ is the change in γ necessary to reduce the value of the determinant to zero.

To find $\Delta\gamma$ it is necessary to evaluate the derivative of the dispersion-relation determinant with respect to the propagation constant. Differentiation of the 6X6 determinant is most easily and quickly done numerically. The procedure followed in evaluating the derivative numerically, point F, Fig. 2, is as follows:

(a) Compute $\gamma_2 = \gamma + 10^{-7}$,

(b) evaluate the dispersion-relation determinant at γ_2 and store the value in $\mathrm{Det}(\gamma_2)$,

(c) evaluate the derivative by using $\frac{\partial \mathrm{Det}(\gamma)}{\partial \gamma} = \frac{\mathrm{Det}(\gamma_2) - \mathrm{Det}(\gamma)}{10^{-7}\gamma}$

The change in γ necessary to reduce the value of the dispersion-relation determinant to zero is found by solving Eq. (24) for $\Delta\gamma$; one finds

$$\Delta\gamma = -\mathrm{Det}(\gamma) \Big/ \frac{\partial \mathrm{Det}(\gamma)}{\partial \gamma} .$$

At point G, Fig. 2, a decision must be made by the program; if the computed fractional change in γ is greater than 0.0001, a new γ

is calculated at H, and the program returns through I to junction D. At I, a counter is indexed which counts the number of times γ has been calculated. A solution usually requires two to four iterations. If the above process is repeated too many times (eight is the maximum number of iterations allowed in this program), the program is terminated and a set of error messages is printed. This usually occurs if an improbable set of independent variables has been submitted for analysis.

If the computed fractional change in γ is less than 0.0001, the determinantal equation is said to be satisfied, and the program proceeds to calculate other properties of the hollow plasma waveguide. If the programmer requested, via the input data, plots of the axial electric field as a function of radial position, it is necessary to determine the coefficients of the Bessel functions in the field expressions of Eqs. (18) and (19) and Appendix A. This is accomplished by use of a subroutine that evaluates ratios of five of the coefficients to the sixth.[22] After the coefficient ratios have been calculated, point J on Fig. 2, the field in any region of the plasmaguide may be expressed as a percentage of the axial electric field at the center line of the plasmaguide.

The wall losses may now be calculated by a perturbation technique discussed in Chapter V. Just as for the axial electric field plots, the wall loss calculations are optional, depending upon the choice of the programmer via the data input.

At point K, the results of the calculation up to now are stored in a form suitable for punching, upon completion of the program, a set of output data cards containing the propagation characteristics

and field plot data. The program, at point L, of Fig. 2, then proceeds to increment the rf frequency, test if the new frequency is less than the desired maximum frequency ω_{max}, and return to point M to determine a new propagation constant at the new rf frequency, etc.

After the propagation constants for a series of frequencies up to a value three times the cutoff frequency have been determined, the program will return from point N to point O if there is another set of plasmaguide independent variables to process. If there are no more input data cards, a tabulation of the calculations is printed and a set of output data is punched by the card punch associated with the digital computer. These output data cards are used to plot the characteristics of several plasmaguide designs on the same graph, as shown in Figs. 3 through 16.

IV. CUTOFF

At the cutoff frequency, ω_0, of the hollow plasma waveguide, there is no energy propagation in the axial direction ($\beta = 0$). Referring to the auxiliary quantities defined in the discussion of the plasma region field equations (Eqs. 9 to 12), it may be seen that, at cutoff

$$a_1 = \frac{\epsilon_{11}^2 - \epsilon_{12}^2}{\epsilon_{11}} k^2,$$

$$a_2 = \epsilon_{33} k^2,$$

$$b_1 = 0,$$

$$b_2 = 0.$$

For b_1 and b_2 equal to zero, the TE and TM modes are uncoupled, as may be seen by referring to the scalar wave Eqs. (13) and (14). Considering only the TM mode, the scalar wave equation for the axial electric field at cutoff is

$$(\nabla_T^2 + a_2) E_z = 0. \tag{26}$$

For the case of $\omega_p > \omega$, we find $a_2 < 0$. Therefore, solutions of the scalar wave equation in the plasma region are linear combinations of modified Bessel functions of the first and second kinds. The axial electric field in the plasma region is given by

$$E_z = AI_0(T_c r) + BK_0(T_c r), \tag{27}$$

where $T_c = \sqrt{-\epsilon_{33} k^2}$, and I_0 and K_0 are the modified Bessel functions of the first and second kinds.

To determine the cutoff frequency of the plasmaguide, it is necessary to derive expressions for the rest of the cutoff fields. The boundary conditions at cutoff are similar to those required for the general solution of the plasmaguide dispersion relation; see Chapter III.

The required field expressions may easily be derived from the general plasmaguide field expressions by letting $\beta = 0$ and using Eq. (27) for the axial electric field in the plasma region:

$$H_\theta = iT_c[AI_1(T_c r) - BK_1(T_c r)]/k\eta \quad \text{(plasma region at cutoff)}, \quad (28)$$

$$E_z^v = CJ_0(kr) \quad \text{(vacuum region at cutoff)}, \quad (29)$$

$$H_\theta^v = -iCJ_1(kr)/\eta \quad \text{(vacuum region at cutoff)}. \quad (30)$$

At cutoff, the resultant determinantal equation that must be solved for the hollow plasma waveguide cutoff frequency is

$$\begin{vmatrix} a_{11} & a_{12} & a_{13} \\ a_{21} & a_{22} & a_{23} \\ a_{31} & a_{32} & 0 \end{vmatrix} = 0,$$

where

$a_{11} = I_0(T_c R_0)$, $a_{12} = K_0(T_c R_0)$, $a_{13} = -J_0(kR_0)$,

$a_{21} = L_c I_1(T_c R_0)$, $a_{22} = -L_c K_1(T_c R_0)$, $a_{23} = +iJ_1(kR_0)/\eta$,

$a_{31} = I_0(T_c R_w)$, $a_{32} = K_0(T_c R_w)$, and $L_c = iT_c/k\eta$.

Solution of the cutoff determinantal dispersion relation is performed numerically, point B on the logical flow chart of Fig. 2, by the same method as used to find the γ necessary to satisfy the general dispersion relation; see the "Method of Solution" discussion in Chapter III. In the numerical method of solution, a first guess at the cutoff frequency is needed. The first guess is obtained by using the approximation for the cutoff frequency of a hollow plasma waveguide with the same vacuum radius but with a infinite outer conductor radius as derived by August.[2] For ω_p/ω_0 greater than 3.0,

August has derived the expression

$$\omega_0 = \omega_0'(1 - c/\omega_p R_0),$$

where ω_0' = the TM_{01} mode cutoff frequency of a round metal guide with a radius equal to the vacuum region radius.

It may be noted that all the elements of the cutoff determinantal dispersion relation are independent of the axial magnetic field. Therefore the cutoff frequencies for the TM modes are independent of the axial magnetic field.

V. ATTENUATION DUE TO FINITE WALL CONDUCTIVITY

1. Perturbation Technique

In specifying the boundary conditions for the hollow plasma waveguide, Chapter III, the tangential electric fields at the metal wall of the outer conductor were set equal to zero. Even for very good conductors, a small tangential electric field exists; however, the field distribution is only slightly perturbed from the loss-free solution.

By the perturbation technique described by Stratton, the loss-free solution is used to approximate the tangential magnetic fields at the conductor surface.[23] Assuming the conduction current in the wall is very much greater than the displacement current (always true, by definition, for a good conductor), the surface current density in the wall is given by

$$\vec{J}_s = \vec{n} \times \vec{H}_t .$$

The average power dissipated per unit length in the walls is given by

$$P_l = \frac{R_s}{2} \oint_s |\vec{J}_s|^2 \, ds ,$$

where R_s is the surface resistivity of the wall in ohms per square. R_s used in the calculation is, at room temperature, $2.61 \times 10^{-7} \sqrt{f}$ ohms for copper;[24] f is the rf frequency in Hz.

To determine the attenuation constant due to the effect of finite wall conductivity, point P on Fig. 2, one must first determine the total energy flow in the axial direction. The time-average axial energy flow calculations are carried out with the plasma losses set equal to zero; $\nu = 0$.

2. Time-Average Axial Power Flow

(a) Vacuum Region: $0 \leq r \leq R_o$

The time-average axial vacuum power flow is given by

$$P_v = \int_0^{2\pi} d\theta \int_0^{R_o} S^v r\,dr, \tag{32}$$

where $S^v = (1/2)\,\mathrm{Re}(E_r^v H_\theta^{v*} - E_\theta^v H_r^{v*})$

Note: A starred quantity indicates the complex conjugate of the quantity.

From the transverse field equations, Appendix A, we find

$$E_r^v H_\theta^{v*} = \frac{\mathcal{A}\beta}{K4\eta} C^2 Q_o'^2(T_3 r),$$

and $$-E_\theta^v H_r^{v*} = \frac{\mathcal{A}\beta}{K4\eta} D^2 Q_o'^2(T_3 r).$$

Therefore, $$S^v = \frac{1}{2}\frac{\mathcal{A}\beta}{K4\eta}(C^2 + D^2)\, Q_o'^2(T_3 r) \tag{33}$$

and $$P_v = \frac{\pi \mathcal{A}\beta}{K4\eta}(C^2 + D^2)\int_0^{R_o} r\, Q_o'^2(T_3 r)\,dr. \tag{34}$$

The definite integral expression used to evalute the time-average axial vacuum power flow expression is given in Appendix C for both unmodified and modified Bessel's functions.

(b) Plasma Region: $R_o \leq r \leq R_w$

The time-average axial plasma power flow is given by

$$P_p = \int_0^{2\pi} d\theta \int_{R_o}^{R_w} S^p r\,dr, \tag{35}$$

where $S^p = (1/2)\,\mathrm{Re}(E_r H_\theta^* - E_\theta H_r^*)$.

Using the expressions for the transverse plasma fields given in Appendix A, we find

$$E_r H_\theta^* = \sum_{j=1}^{2} L_{j1} T_j (i L_{j4} T_j)^* \left[A_j Q_o'(T_j r) + B_j W_o'(T_j r)\right] \times \left[A_j Q_o'(T_j r) + B_j W_o'(T_j r)\right]^* \tag{36}$$

and $$-E_\theta H_r^* = -\sum_{j=1}^{2} i L_{j2} T_j (L_{j3} T_j)^* \left[A_j Q_o'(T_j r) + B_j W_o'(T_j r)\right] \times \left[A_j Q_o'(T_j r) + B_j W_o'(T_j r)\right]^*. \tag{37}$$

The integral expression for the time-average axial plasma power flow is evaluated by substituting the expressions of Eqs. (36) and (37) into Eq. (35) and performing the indicated integration by numerical means. A numerical integration subroutine developed by Vardas[25] is used to evaluate Eq. (35).

The total time-average axial power flow, P_z, is the sum of two components, the time-average axial power flow in the vacuum region, P_v, and the time-average axial power flow in the plasma region, P_p:

$$P_z = P_v + P_p.$$

3. Time-Average Power Loss in the Wall

The surface current density in the wall is given by

$$J_\theta = H_z\Big|_{r=R_w} = \sum_{j=1}^{2} \frac{F_j}{\eta}\left[A_j Q_o(T_j R_w) + B_j W_o(T_j R_w)\right]$$

and

$$J_z = H_\theta\Big|_{r=R_w} = \sum_{j=1}^{2} i L_{j4} T_j\left[A_j Q_o'(T_j R_w) + B_j W_o'(T_j R_w)\right].$$

The time-average power loss per unit length in the wall is the sum of two components, one due to the small H_z field in the plasma region at the wall, and the other due to the H_θ field in the plasma region at the wall. The loss due to the H_z component at the wall may be neglected with respect to the loss due to the H_θ component. The loss is proportional to the square of the magnitude of the tangential magnetic field. H_θ is typically several powers of ten greater than H_z. Over the range of plasmaguide parameters considered (see Section 1 of Chapter VI), the ratio of the axial magnetic field to the axial electric field varied from 0.0001 to 0.001. The mode of wave

propagation is predominantly transverse magnetic (as defined in Section 2 of Chapter II). The time-average power loss in the wall is given by

$$P_\ell = \sum_{j=1}^{2} \pi R_w R_s \left| L_{j4} T_j \left[A_j Q_o'(T_j R_w) + B_j W_o'(T_j R_w) \right] \right|^2 . \qquad (38)$$

4. Attenuation Constant

The attenuation constant, due to finite conductivity in the walls, α_w, is given by Stratton,[23]

$$\alpha_w = P_\ell / 2P_z . \qquad (39)$$

If the plasma region has losses, $\nu \neq 0$, the γ necessary to satisfy the dispersion relation equation is a complex number (see Chapter III, Section 2). The real part of γ is the attenuation constant due to the losses in the plasma region, α_p. The attenuation constant, α, for a hollow plasma waveguide with walls of finite conductivity and a nonzero collision frequency in the plasma region is given by the sum of the two attenuation constants,

$$\alpha = \alpha_w + \alpha_p .$$

VI. DISCUSSION OF RESULTS

1. Selection of Parameters

The operation of the hollow plasma waveguide may be compared with that of a metal waveguide. In a metal waveguide, electromagnetic energy is reflected at the walls by induced conduction currents; in a hollow plasma waveguide, electromagnetic energy is reflected at the plasma interface by induced currents that are reactive for a lossless plasma. In a metal, the rf frequency is very much less than the electron collision frequency inside the metal, while in a plasma, the reverse can be true. A metal has very small skin depths at rf frequencies; a plasma with $\omega_p > \omega$ may have skin depths several thousand times as large as the metal. The confinement properties are in fact independent of the collision frequency. A low-loss hollow plasma waveguide design will maintain the plasma frequency greater than the rf frequency, $\omega_p > \omega$, and the rf frequency very much greater than the collision frequency, $\omega \gg \nu$.

The other independent variables to be selected are the magnitude of the external axial magnetic field, the outer conductor radius, and the vacuum radius. The size of the vacuum radius is determined by the rf frequency the plasmaguide is designed to carry; see the suggested design at the end of this section. The losses caused by the conduction currents in the outer conductor should be kept small. To ensure this, the ratio of the outer conductor radius to the vacuum radius must be large enough so the rf fields that penetrate through the plasma region to the outer conductor wall are sufficiently attenuated by the intervening plasma volume.

The selection of the magnitude of the external axial magnetic field is difficult because of the complexity of the hollow plasma waveguide dispersion relation equation. The calculation of a propagation characteristic, from ω_0 to $3\omega_0$, for one set of independent variables, requires approximately 12 sec of computation time on a CDC 6600 computer, or approximately 50 sec on an IBM 7094 computer. It is economically feasible to try a likely set of independent variables, compute the propagation characteristics, examine the results, and then recompute the propagation characteristics with a modified set of independent variables. One does not have to repeat this procedure too many times before the results described in the following paragraphs are obtained.

2. Results

The phase characteristics obtained for several values of external axial magnetic field, with a ratio of plasma frequency to cutoff frequency of four, is given in Fig. 3. The curves are normalized as discussed in Chapter III, Method of Solution. For purposes of comparison, the TM_{01} mode $\omega-\beta$ diagram is displayed for a metal waveguide with the same TM_{01} mode cutoff frequency as the plasmaguide. This is the equivalent metal guide referred to in Chapter III; R(eq), Fig. 3, is its radius.

The cutoff frequency found for each of the four curves shown is the same, independent of the external axial magnetic field as derived in Chapter IV. The cutoff frequency for this ratio of plasma frequency to cutoff frequency is 12% lower than the TM_{01} mode cutoff frequency of a metal guide with the same radius as the vacuum region radius.

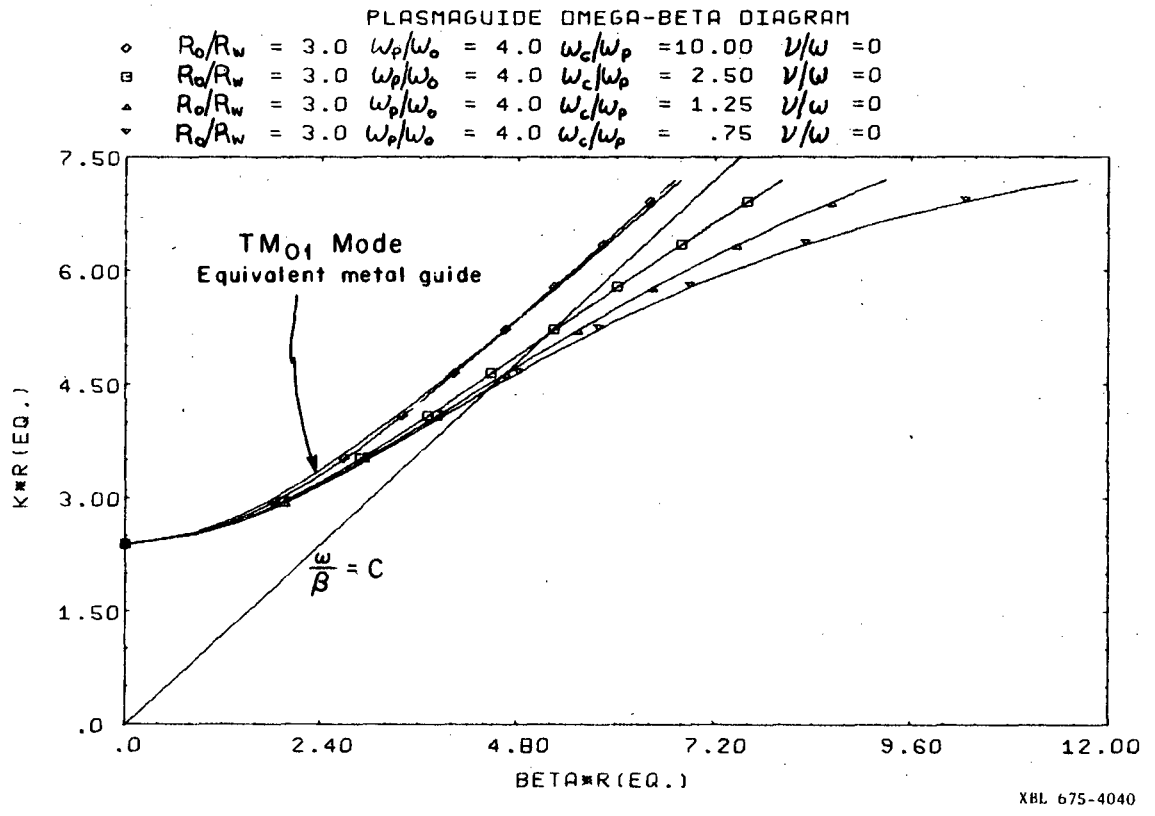
PLASMAGUIDE OMEGA-BETA DIAGRAM
R_o/R_w = 3.0 ω_p/ω_o = 4.0 ω_c/ω_p =10.00 ν/ω =0
R_o/R_w = 3.0 ω_p/ω_o = 4.0 ω_c/ω_p = 2.50 ν/ω =0
R_o/R_w = 3.0 ω_p/ω_o = 4.0 ω_c/ω_p = 1.25 ν/ω =0
R_o/R_w = 3.0 ω_p/ω_o = 4.0 ω_c/ω_p = .75 ν/ω =0
TM_{01} Mode
Equivalent metal guide
$\frac{\omega}{\beta} = C$
K*R(EQ.)
BETA*R(EQ.)
7.50
6.00
4.50
3.00
1.50
.0
.0
2.40
4.80
7.20
9.60
12.00
XBL 675-4040

Fig. 3

The phase and group velocity curves corresponding to the ω-β diagrams of Fig. 3 are shown in Figs. 4, 5, and 6. The velocity at which an equiphase surface travels is called the phase velocity of the wave. It is given by

$$V_p = \frac{k}{\beta} \quad .$$

Therefore, the ratio of the ordinate to the abscissa of the ω- β diagrams of Fig. 3 is the phase velocity of the wave in the plasmaguide. The velocity of propagation of energy, the group velocity, is given by

$$V_g = \left(\frac{d\beta}{dk}\right)^{-1} \quad .$$

The group velocity is the reciprocal of the derivative of the ω-β diagram. The derivative of the ω- β diagram is obtained numerically. The phase and group velocity curves shown in Figs. 4, 5, and 6 are normalized with respect to the speed of light in a vacuum.

The ω- β diagram for a plasmaguide with a very large external axial magnetic field (ω_c/ω_p = 10.0, on Fig. 3) very closely resembles that of the equivalent metal waveguide. The character of the solutions of the dispersion relation, Eq. (23), changes as the external axial magnetic field is decreased. The resulting TM wave phase velocity becomes less than the velocity of light in a vacuum (a slow wave). The change in the ω-β diagram caused by lowering the external axial magnetic field is shown by the three curves for ω_c/ω_p ratios of 2.5, 1.25, and 0.75 on Fig. 3.

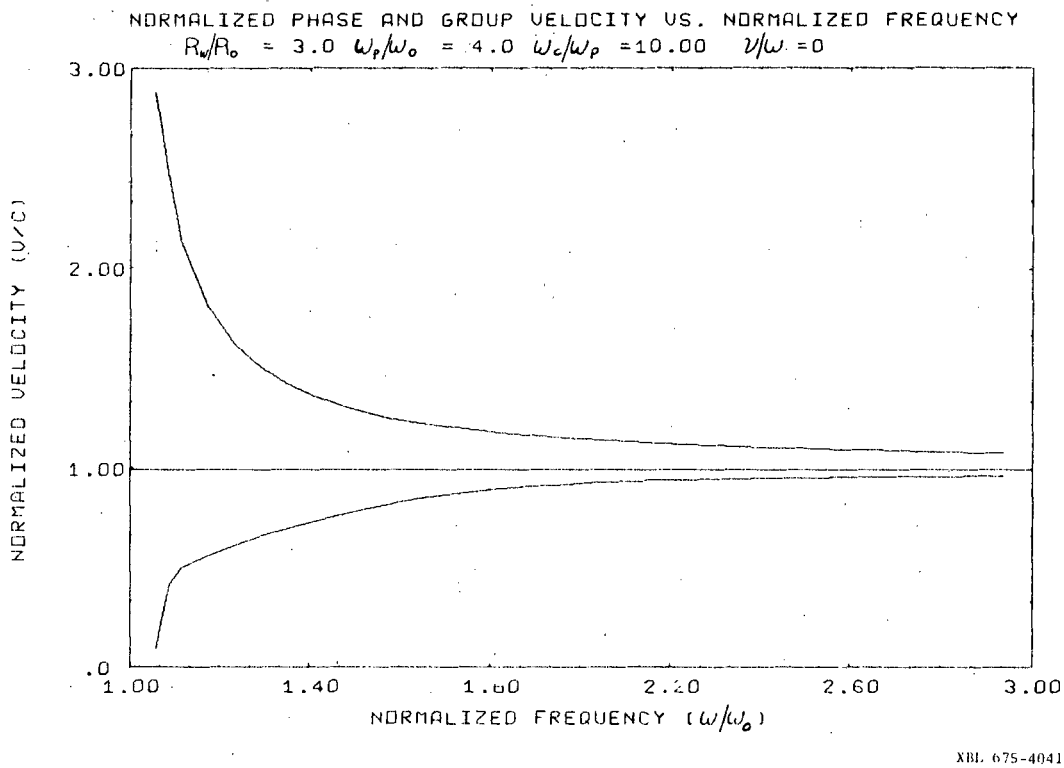
NORMALIZED PHASE AND GROUP VELOCITY VS. NORMALIZED FREQUENCY
R_w/R_o = 3.0 ω_p/ω_o = 4.0 ω_c/ω_p =10.00 ν/ω =0
NORMALIZED VELOCITY (V/C)
3.00
2.00
1.00
.0
1.00
1.40
1.80
2.20
2.60
3.00
NORMALIZED FREQUENCY (ω/ω_o)
XBL 675-4041

Fig. 4

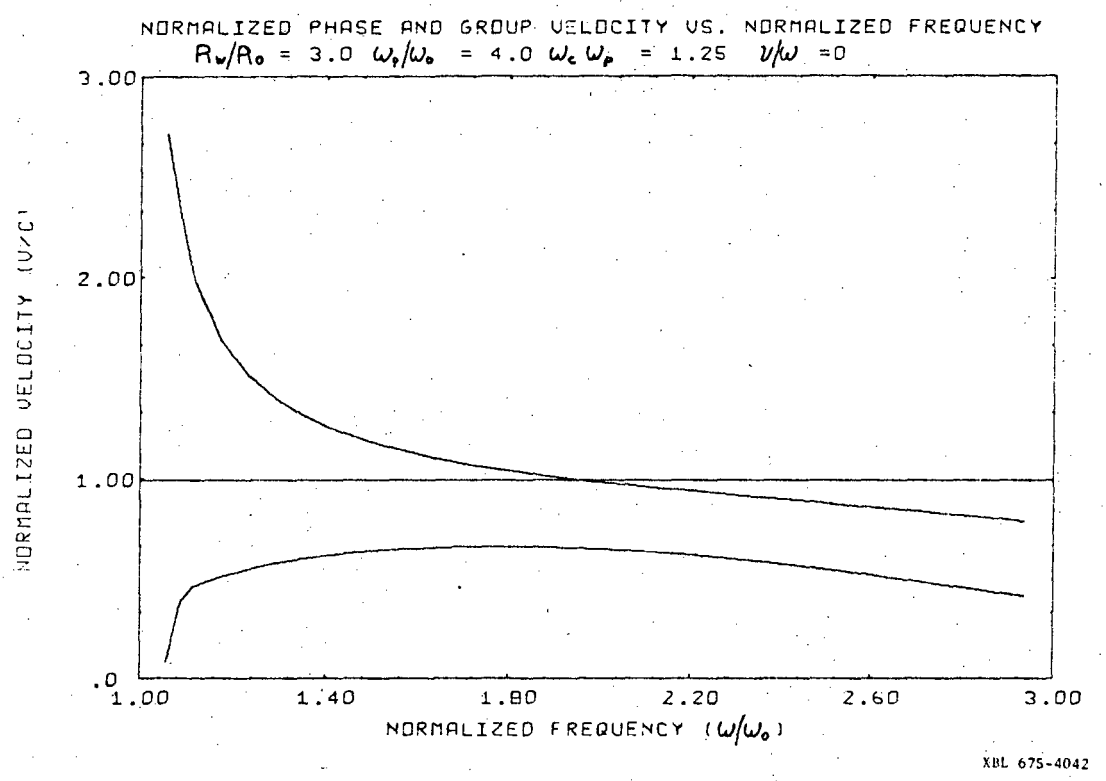
NORMALIZED PHASE AND GROUP VELOCITY VS. NORMALIZED FREQUENCY
R_w/R_0 = 3.0 ω_p/ω_0 = 4.0 $\omega_c\,\omega_p$ = 1.25 ν/ω =0
NORMALIZED VELOCITY (V/C)
3.00
2.00
1.00
.0
1.00
1.40
1.80
2.20
2.60
3.00
NORMALIZED FREQUENCY (ω/ω_0)
XBL 675-4042

Fig. 5

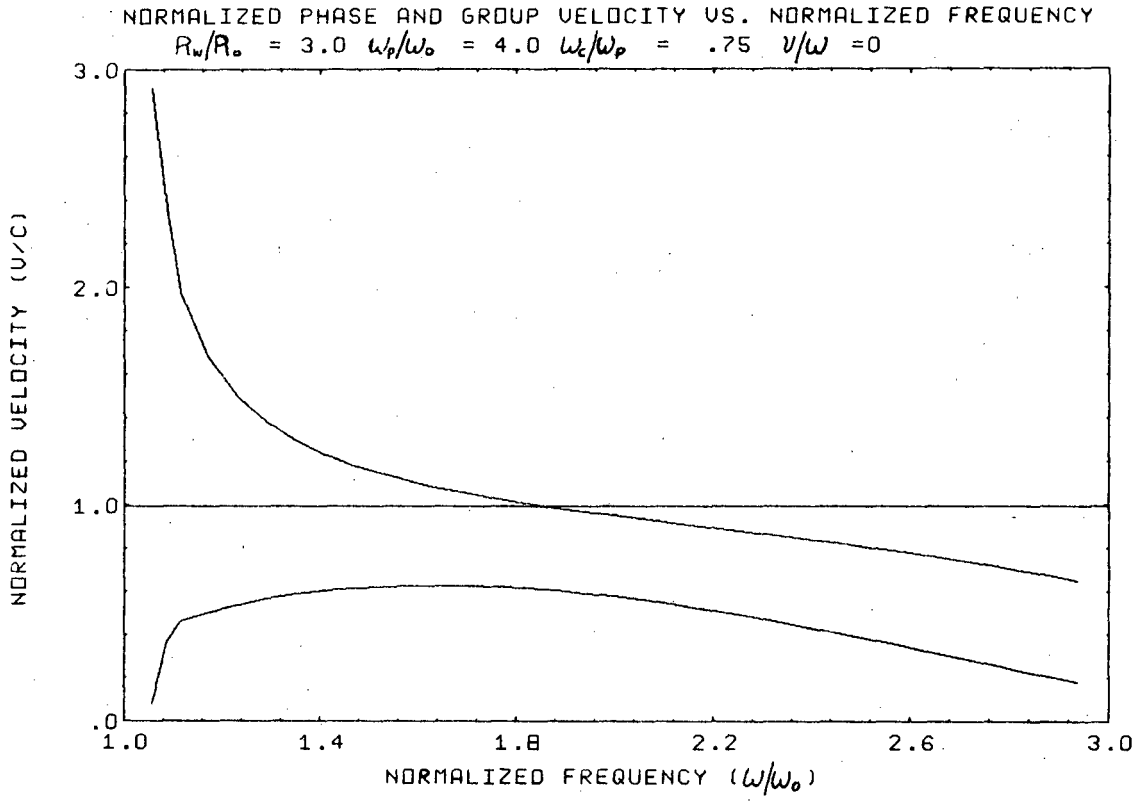
NORMALIZED PHASE AND GROUP VELOCITY VS. NORMALIZED FREQUENCY
R_w/R_o = 3.0 ω_p/ω_o = 4.0 ω_c/ω_p = .75 ν/ω =0
NORMALIZED VELOCITY (V/C)
3.0
2.0
1.0
.0
1.0
1.4
1.8
2.2
2.6
3.0
NORMALIZED FREQUENCY (ω/ω_o)
XBL 675-4043

Fig. 6

The extent of penetration of the electromagnetic fields into the plasma region may be seen from the plots of axial electric field versus radial position shown in Figs. 7, 8, and 9, with $\omega_c/\omega_p = 1.25$ and varying ω/ω_0. It may be seen from the set of axial electric field distribution curves that the axial electric field decays to a very small value at an appreciable distance from the outer conductor wall. This suggests that the choice of the ratio of the outer conductor radius to vacuum radius, for this set of field plots, is larger than necessary for a low-loss waveguide.

For slow wave solutions, the highest axial electric field is found at the plasma-vacuum interface. Figure 8 shows the axial electric field distribution for a plasmaguide with a normalized phase velocity just slightly less than unity ($V_p = 0.99$, $\omega/\omega_0 = 2.0$). The axial electric field at the plasma-vacuum interface is only slightly higher than the axial electric field along the plasmaguide center line. If the rf frequency is increased, the axial electric field at the plasma-vacuum interface becomes very large and the phase velocity of the TM mode wave decreases ($V_p = 0.76$, $\omega/\omega_0 = 3.0$); see Fig. 9.

Large fields at the plasma-vacuum interface extend further into the plasma region and cause the attenuation of the plasmaguide to increase very rapidly as the phase velocity of the plasmaguide decreases. Figure 10 is a plot of the ratio of the plasmaguide attenuation to an equivalent metal guide attenuation for several values of electron-ion collision frequency in the plasma region. It may be noted that a large improvement in the attenuation of the plasmaguide, compared with the attenuation of the equivalent metal guide, may still be achieved even for the slow-wave

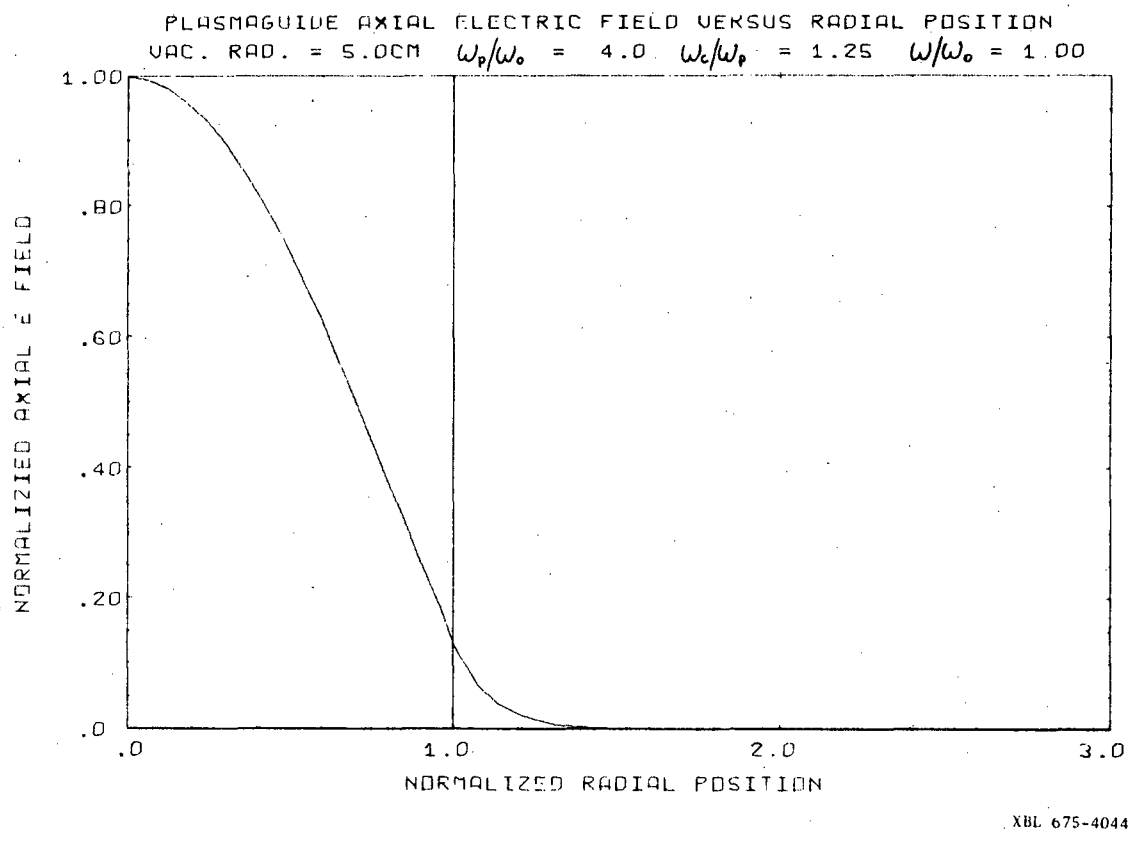
PLASMAGUIDE AXIAL ELECTRIC FIELD VERSUS RADIAL POSITION
VAC. RAD. = 5.0CM ω_p/ω_o = 4.0 ω_c/ω_p = 1.25 ω/ω_o = 1.00
NORMALIZIED AXIAL E FIELD
1.00
.80
.60
.40
.20
.0
.0
1.0
2.0
3.0
NORMALIZED RADIAL POSITION
XBL 675-4044

Fig. 7

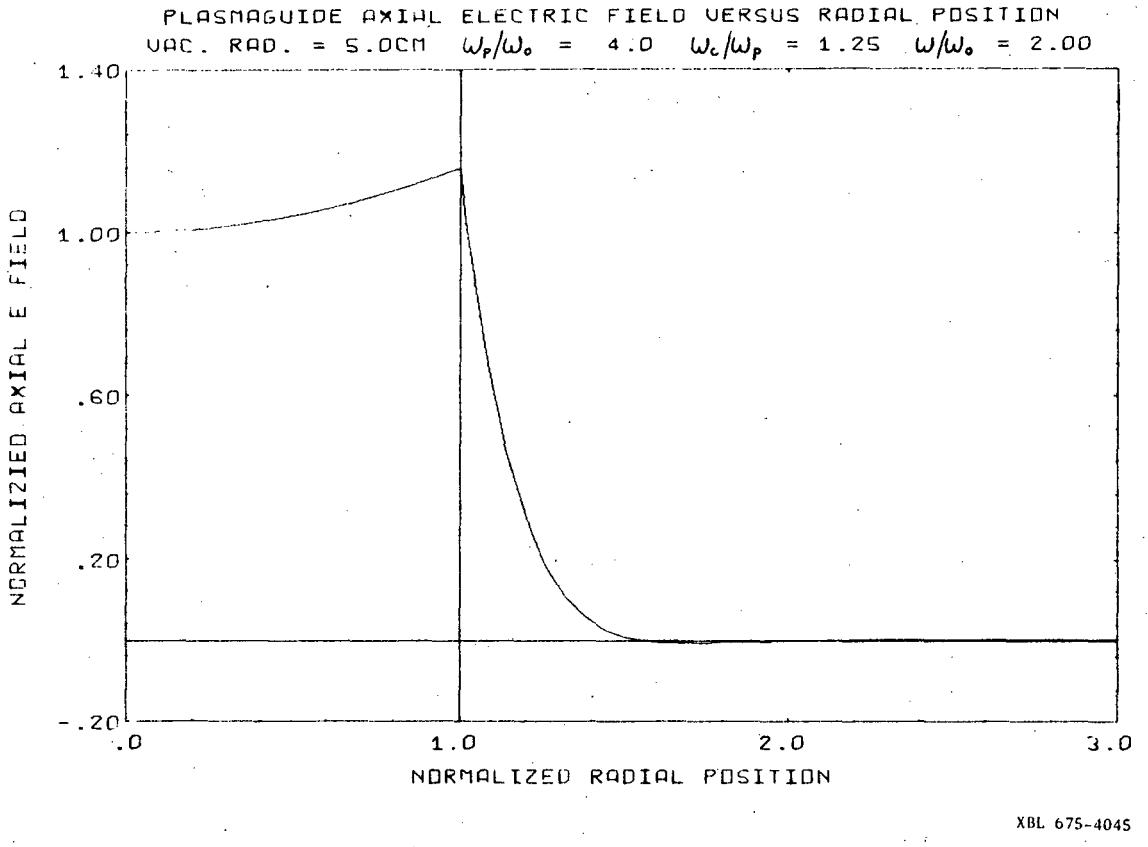
PLASMAGUIDE AXIAL ELECTRIC FIELD VERSUS RADIAL POSITION
VAC. RAD. = 5.0CM ω_p/ω_o = 4.0 ω_c/ω_p = 1.25 ω/ω_o = 2.00
NORMALIZIED AXIAL E FIELD
1.40
1.00
.60
.20
-.20
.0
1.0
2.0
3.0
NORMALIZED RADIAL POSITION
XBL 675-4045

Fig. 8

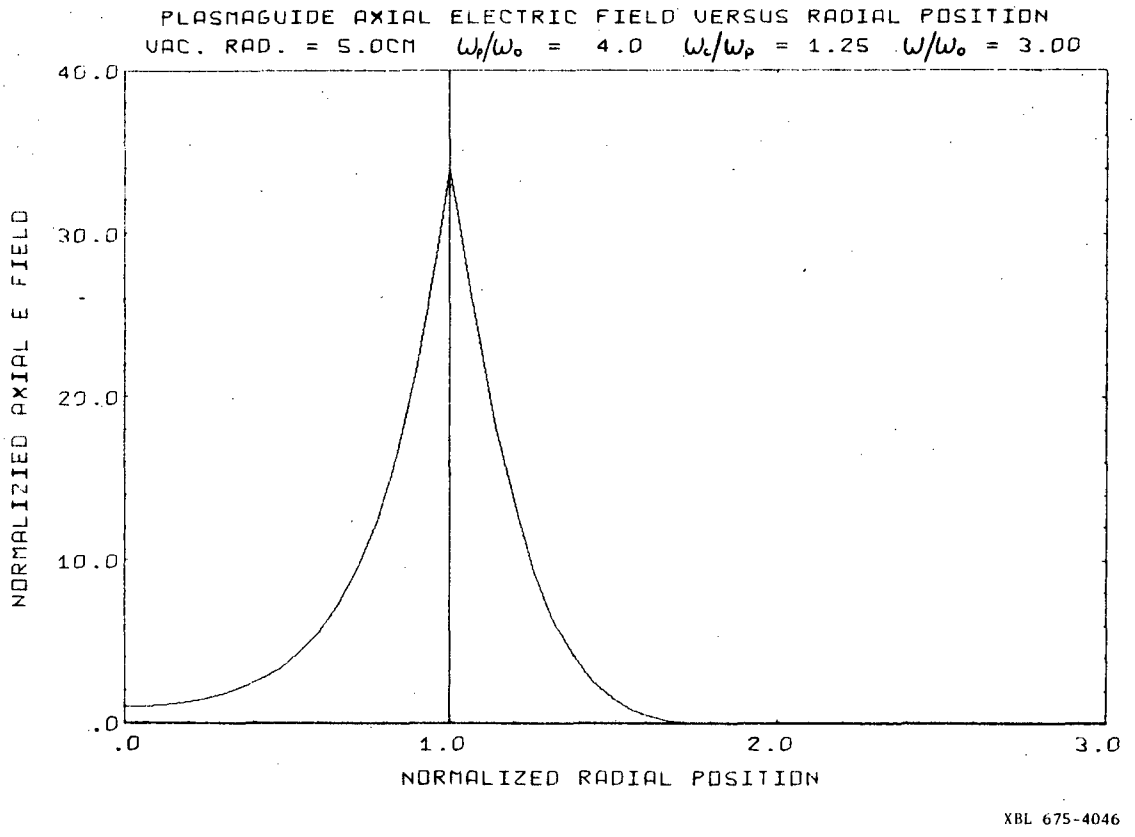
PLASMAGUIDE AXIAL ELECTRIC FIELD VERSUS RADIAL POSITION
VAC. RAD. = 5.0CM ω_p/ω_o = 4.0 ω_c/ω_p = 1.25 ω/ω_o = 3.00
NORMALIZIED AXIAL E FIELD
40.0
30.0
20.0
10.0
.0
.0
1.0
2.0
3.0
NORMALIZED RADIAL POSITION
XBL 675-4046

Fig. 9

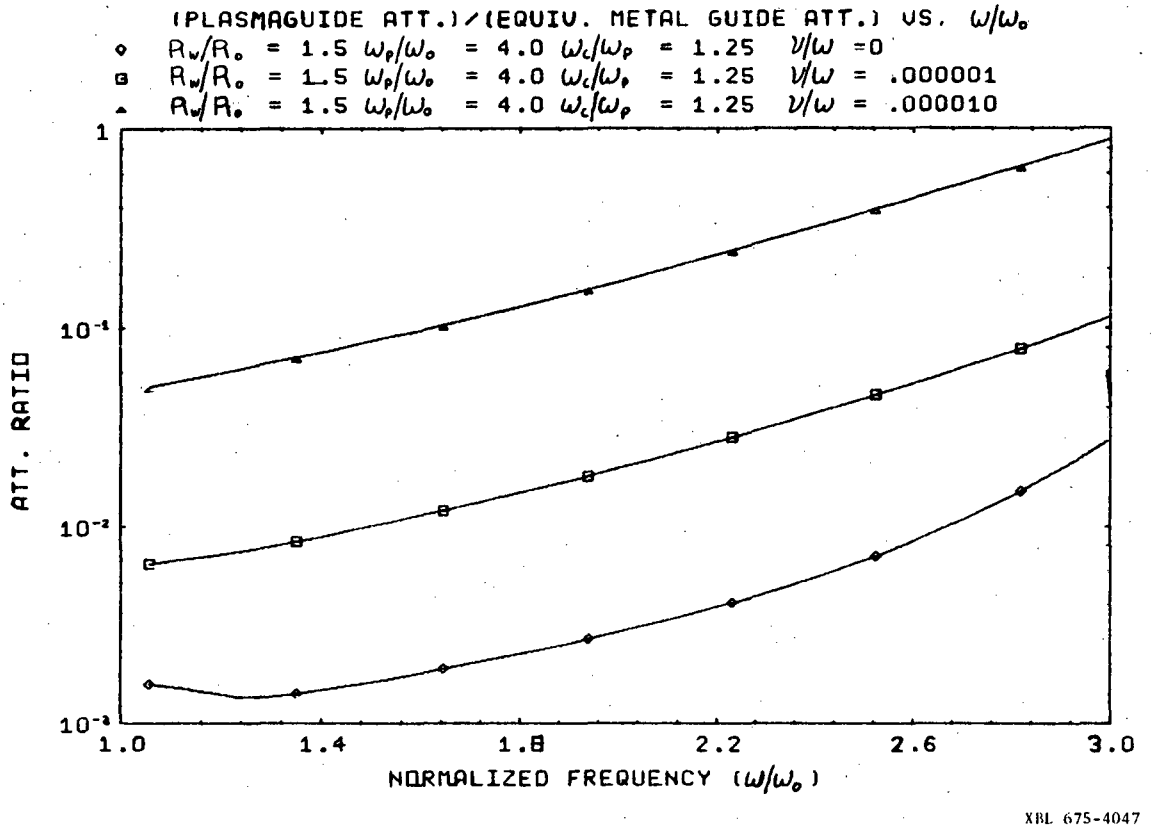
(PLASMAGUIDE ATT.)/(EQUIV. METAL GUIDE ATT.) VS. ω/ω₀
◇ Rw/R₀ = 1.5 ωp/ω₀ = 4.0 ωc/ωp = 1.25 ν/ω = 0
□ Rw/R₀ = 1.5 ωp/ω₀ = 4.0 ωc/ωp = 1.25 ν/ω = .000001
△ Rw/R₀ = 1.5 ωp/ω₀ = 4.0 ωc/ωp = 1.25 ν/ω = .000010
ATT. RATIO
1
10⁻¹
10⁻²
10⁻³
1.0
1.4
1.8
2.2
2.6
3.0
NORMALIZED FREQUENCY (ω/ω₀)
XBL 675-4047

Fig. 10

portion of the propagation characteristics. The attenuation rises rapidly as the phase and group velocities become very slow. The phase and group velocity curves are shown in Fig. 11 for the plasma-guide of Fig. 10. There is no change in the $\omega - \beta$ diagram, or in the phase and group velocity curves, between the $\nu = 0$ case and the case of small but finite collision frequencies in the plasma volume. Figure 12 shows the attenuation in nepers/m for one of the plasmaguide designs of Fig. 10; also shown for comparison purposes is the attenuation of the equivalent metal guide.

Figure 13 illustrates the effect of varying two of the plasmaguide independent variables. The attenuation ratios shown in Fig. 13 are due only to wall losses; the collision frequency in the plasma volume is set equal to zero. If the ratio of the outer conductor radius to vacuum radius is chosen as 3.0 and 1.5 respectively, the lower and upper attenuation curves of Fig. 13 are produced, demonstrating that a reduction in wall losses by a factor of almost 10^3 may still be achieved with a comparatively thin plasma sheath surrounding the vacuum region. Raising the ratio of the plasma frequency to cutoff frequency from 4.0 to 8.0 increases the factor by which the wall attenuation is reduced from 10^3 to 10^5 (see the middle curve of Fig. 13).

Figure 14 is a plot of the attenuation in nepers/m for the equivalent metal guide and the plasmaguide of the upper attenuation ratio curve of Fig. 13. Figure 15 shows the ratio of the real part of the propagation constant to the imaginary part of the propagation constant versus the normalized rf frequency. Figure 16 shows the ratio of the axial power flow in the plasma region to the axial power flow in the

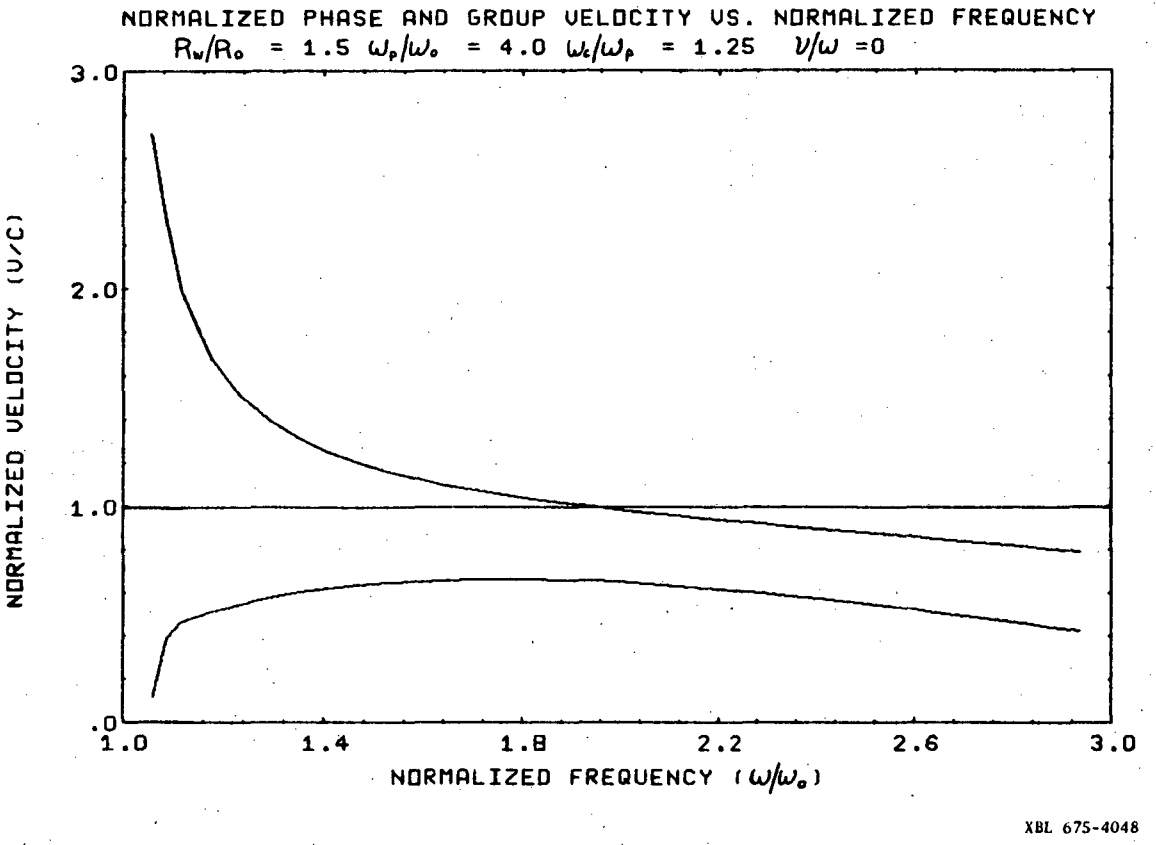
NORMALIZED PHASE AND GROUP VELOCITY VS. NORMALIZED FREQUENCY
R_w/R_o = 1.5 ω_p/ω_o = 4.0 ω_c/ω_p = 1.25 ν/ω =0
NORMALIZED VELOCITY (V/C)
3.0
2.0
1.0
.0
1.0
1.4
1.8
2.2
2.6
3.0
NORMALIZED FREQUENCY (ω/ω_o)
XBL 675-4048

Fig. 11

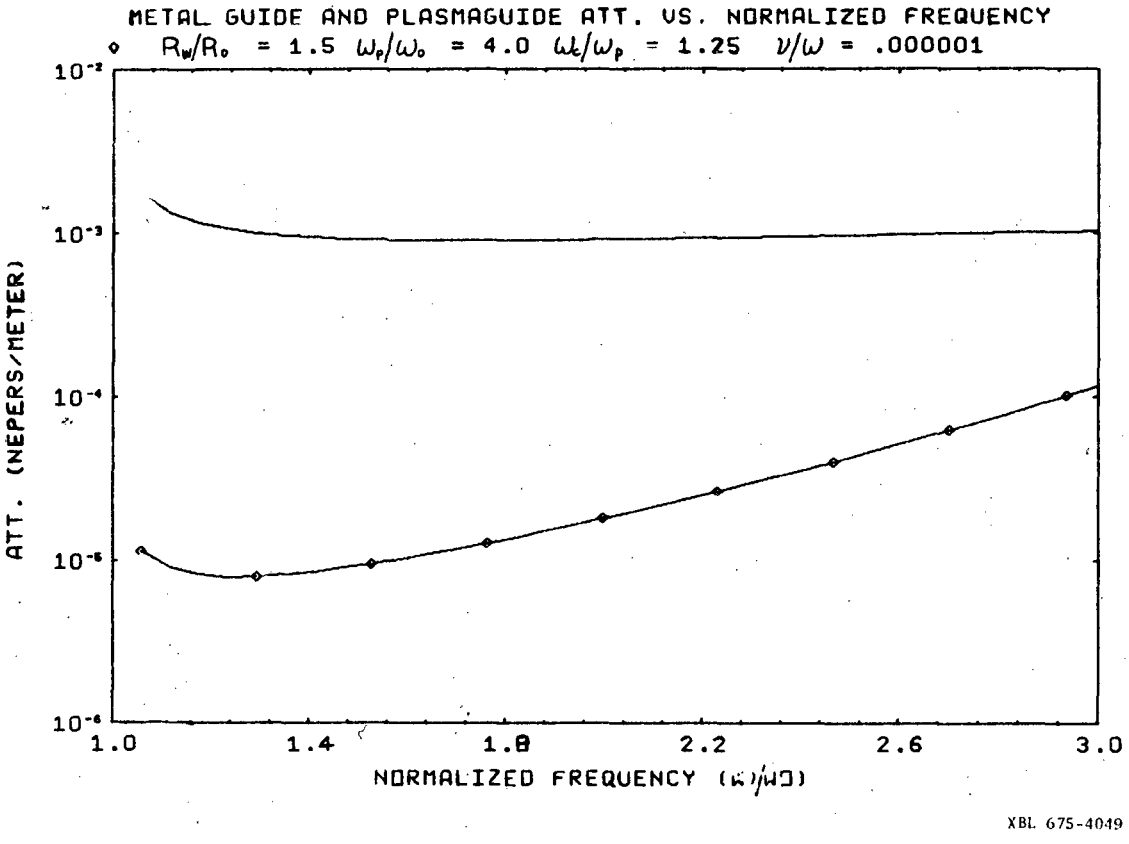
METAL GUIDE AND PLASMAGUIDE ATT. VS. NORMALIZED FREQUENCY
◇ R_w/R_o = 1.5 ω_p/ω_o = 4.0 ω_c/ω_p = 1.25 ν/ω = .000001
ATT. (NEPERS/METER)
10^{-2}
10^{-3}
10^{-4}
10^{-5}
10^{-6}
1.0
1.4
1.8
2.2
2.6
3.0
NORMALIZED FREQUENCY (ω/ωp)
XBL 675-4049

Fig. 12

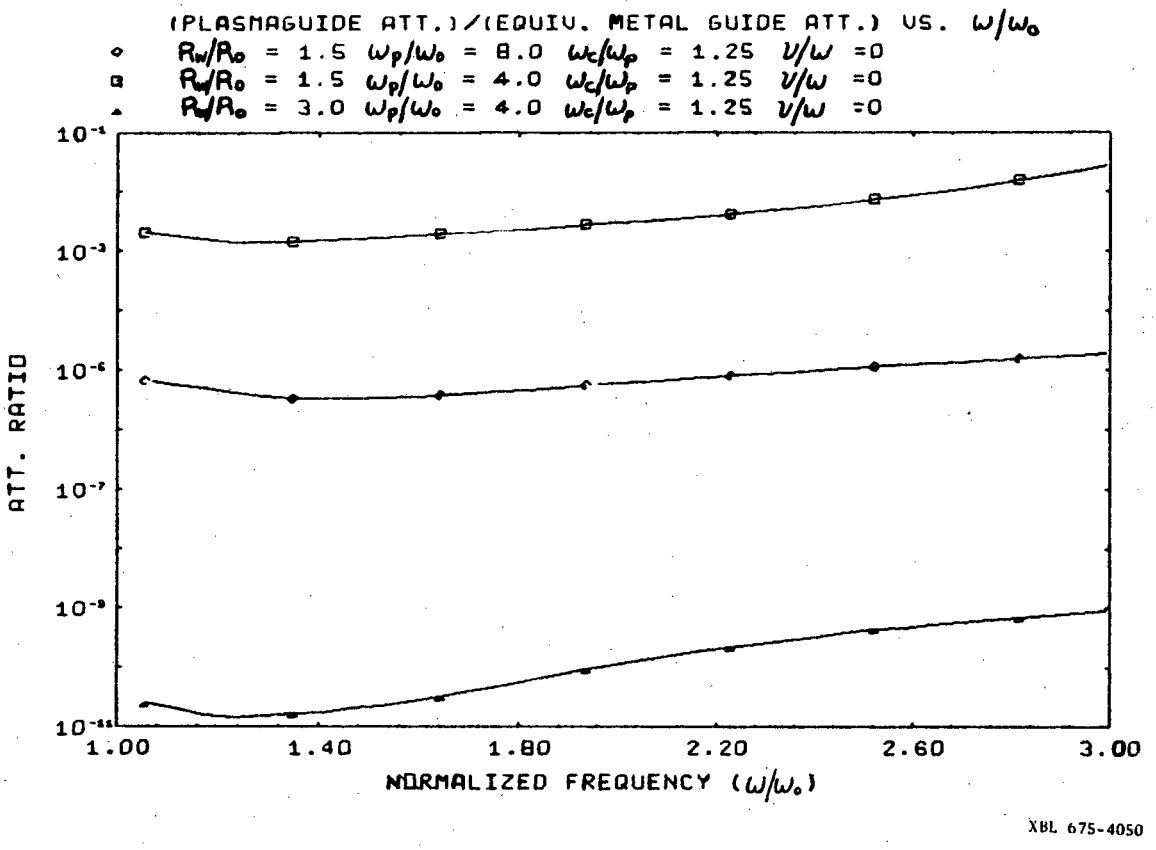
(PLASMAGUIDE ATT.)/(EQUIV. METAL GUIDE ATT.) VS. ω/ω₀
◇ Rw/R0 = 1.5 ωp/ω0 = 8.0 ωc/ωp = 1.25 ν/ω =0
□ Rw/R0 = 1.5 ωp/ω0 = 4.0 ωc/ωp = 1.25 ν/ω =0
△ Rw/R0 = 3.0 ωp/ω0 = 4.0 ωc/ωp = 1.25 ν/ω =0
ATT. RATIO
10⁻¹
10⁻³
10⁻⁵
10⁻⁷
10⁻⁹
1.00
1.40
1.80
2.20
2.60
3.00
NORMALIZED FREQUENCY (ω/ω₀)
XBL 675-4050

Fig. 13

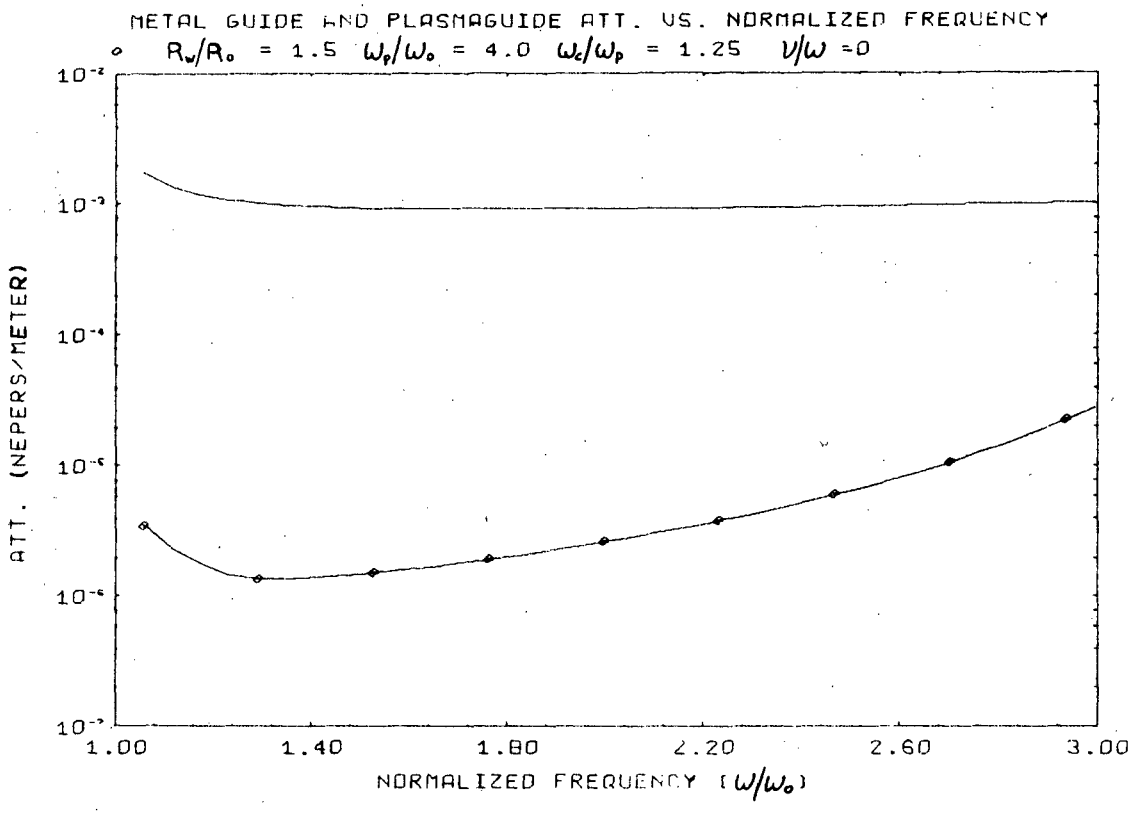
METAL GUIDE AND PLASMAGUIDE ATT. VS. NORMALIZED FREQUENCY
R_w/R_o = 1.5 ω_p/ω_o = 4.0 ω_c/ω_p = 1.25 ν/ω =0
ATT. (NEPERS/METER)
10^{-2}
10^{-3}
10^{-4}
10^{-5}
10^{-6}
10^{-7}
1.00
1.40
1.80
2.20
2.60
3.00
NORMALIZED FREQUENCY (ω/ω_o)
XBL 675-4051

Fig. 14

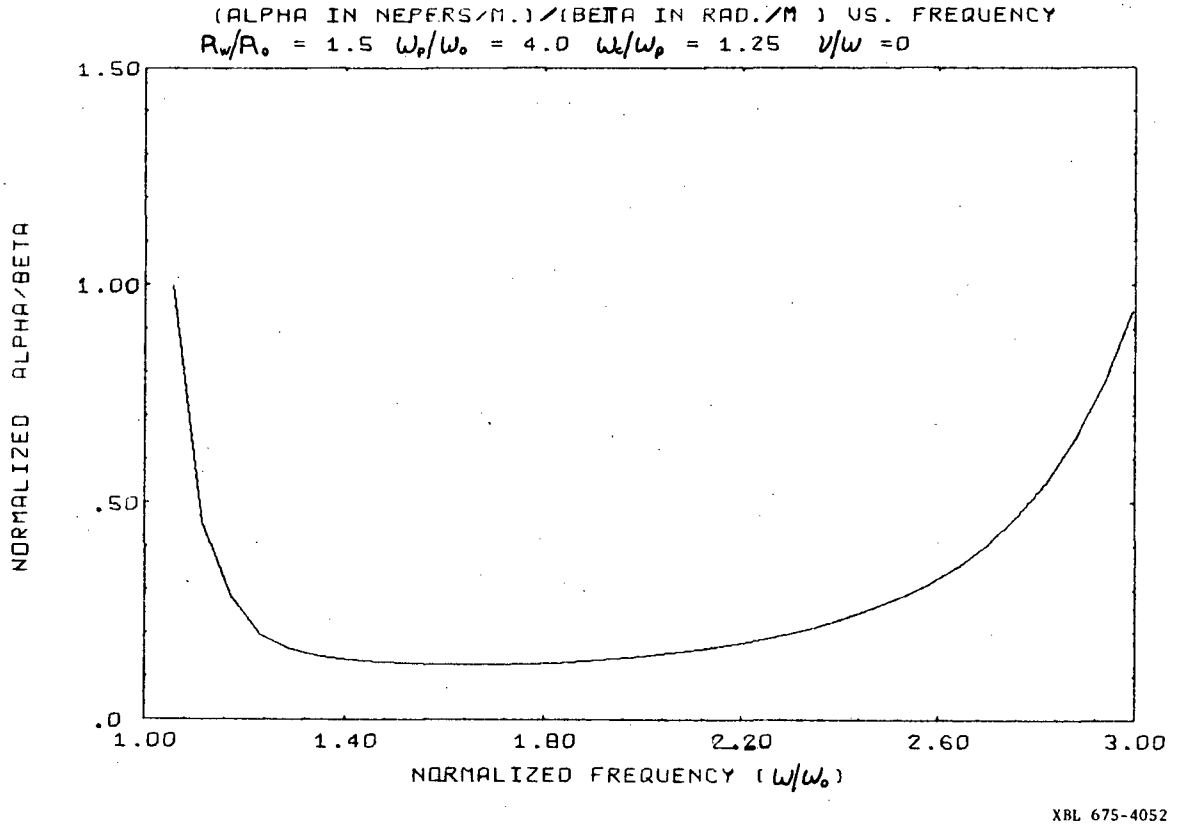
(ALPHA IN NEPERS/M.)/(BETA IN RAD./M) VS. FREQUENCY
R_w/R_o = 1.5 ω_p/ω_o = 4.0 ω_c/ω_p = 1.25 ν/ω =0
NORMALIZED ALPHA/BETA
1.50
1.00
.50
.0
1.00
1.40
1.80
2.20
2.60
3.00
NORMALIZED FREQUENCY (ω/ω_o)
XBL 675-4052

Fig. 15

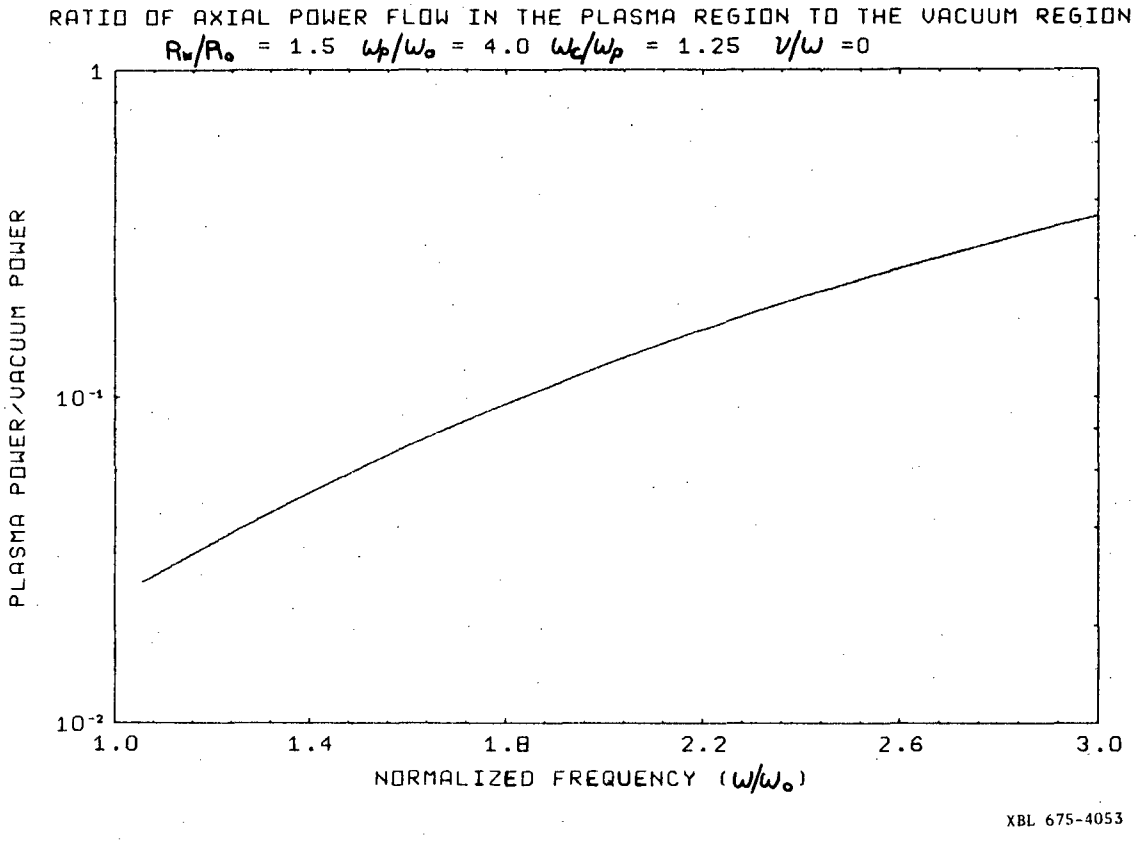
RATIO OF AXIAL POWER FLOW IN THE PLASMA REGION TO THE VACUUM REGION
R_w/R_o = 1.5 ω_p/ω_o = 4.0 ω_c/ω_p = 1.25 ν/ω =0
PLASMA POWER/VACUUM POWER
1
10^{-1}
10^{-2}
1.0
1.4
1.8
2.2
2.6
3.0
NORMALIZED FREQUENCY (ω/ω_o)
XBL 675-4053

Fig. 16

vacuum region versus the normalized frequency. Figures 15 and 16 illustrate the degradation of the plasma containment and consequent rise in attenuation as the rf frequency approaches the plasma frequency.

3. A Suggested Hollow Plasma Waveguide Design

As an illustration of how one may use the curves presented here to evaluate a particular design, the following example is given.

Choosing a vacuum radius of 5 cm as a convenient size (the rf frequency will then be in the 10-cm band), we find the TM mode cutoff frequency, for $\omega_p/\omega_0 = 4.0$, equal to 2.06 GHz. The attenuation ratio curves displayed in Fig. 10 show that for an outer conductor radius of 7.5 cm, the attenuation, for $\nu/\omega = 10^{-6}$, will be approximately 0.018 times that of an equivalent metal guide. The rf frequency used is 4.12 GHz, two times the cutoff frequency; at this rf frequency, the normalized phase velocity is approximately 1.0 (see Fig. 11). The external magnetic field required is 3.68 kG; $\omega_c/\omega_p = 1.25$.

For a fully ionized gas, the plasma frequency required corresponds to a gas pressure of 1.2×10^{-5} mm. For a ratio of collision frequency to rf frequency of 10^{-6}, at $\omega_p = 8.24 \times 10^9$ rad/sec, a 100% ionized hydrogen gas requires an electron temperature of approximately 55 000° K (4.9 eV).

VII. CONCLUSIONS AND SUGGESTIONS FOR FURTHER WORK

Solutions of the dispersion relation for a hollow plasma waveguide with a finite external axial magnetic field may be found by numerical means. Computations of plasmaguide propagation curves and field plots may be performed rapidly on modern high-speed digital computers.

Hollow plasma waveguide designs supporting predominantly transverse magnetic waves with adjustable phase velocities and significantly lower attenuation than comparable metal guides have been demonstrated. The hollow plasma waveguide is a relatively simple structure of uniform cross section. A very modest external axial magnetic field is required. This field performs the dual functions of confining the plasma and of modifying the phase velocity of the TM-mode wave.

It is suggested that further work be carried out on the validity of the dielectric tensor formulation when strong rf fields are present. This formulation may no longer be a meaningful way of describing the electromagnetic properties of the plasma.

Further calculations should be undertaken to determine the effect of plasma density time variations and the effect on the propagation characteristics of the existence of a nonuniform plasma density distribution.

Construction and testing of an experimental hollow plasma waveguide model could proceed concurrently with the further theoretical investigation required.

ACKNOWLEDGMENTS

I want to take this opportunity to express my thanks and appreciation to Professor J. R. Woodyard for his assistance and expert guidance during the course of this research project. The timely advice of Professor A. J. Lichtenberg was essential to the completion of the study.

I would also like to thank Dr. Loren P. Meissner of the Lawrence Radiation Laboratory, Math and Computing Group, for his continued interest in the problem and his many kind suggestions. It should also be noted that G. S. Tool of the Lawrence Radiation Laboratory, Accelerator Study Group, provided many helpful suggestions.

This work was done under the auspices of the U. S. Atomic Energy Commission.

APPENDIX A

Plasma Region Transverse Field Equations

$$E_r = \sum_{j=1}^{2} L_{j1} T_j \left[A_j Q_o'(T_j r) + B_j W_o'(T_j r) \right],$$

$$E_\theta = \sum_{j=1}^{2} i L_{j2} T_j \left[\quad " \quad " \quad \right],$$

$$H_r = \sum_{j=1}^{2} L_{j3} T_j \left[\quad " \quad " \quad \right],$$

$$H_\theta = \sum_{j=1}^{2} i L_{j4} T_j \left[\quad " \quad " \quad \right],$$

$$L_{j1} = \left[i\beta K2 - k^3 \epsilon_{12} F_j \right] / K1,$$

$$L_{j2} = \left[i\beta k^2 \epsilon_{12} - k K2 F_j \right] / K1,$$

$$L_{j3} = \left[k\beta^2 \epsilon_{12} + i\beta K2 F_j \right] / \eta K1,$$

$$L_{j4} = \left[k K3 + i\beta k^2 \epsilon_{12} F_j \right] / \eta K1 .$$

Vacuum Region Transverse Field Equations

$$E_r^v = \frac{i\beta}{T_3} C Q_o'(T_3 r),$$

$$E_\theta^v = \frac{k}{T_3} D Q_o'(T_3 r),$$

$$H_r^v = -\frac{\beta}{T_3 \eta} D Q_o'(T_3 r),$$

$$H_\theta^v = \frac{ik}{T_3 \eta} C Q_o'(T_3 r).$$

Q_0' and W_0' are tabulated for both the unmodified and modified Bessel functions in Appendix C.

APPENDIX B

Dispersion Relation Determinant Elements

In Row 1

From the boundary conditions on E_z at $r = R_0$ we find

$a_{11}=Q_0(T_1R_0)$, $a_{12}=Q_0(T_2R_0)$, $a_{13}=W_0(T_1R_0)$, $a_{14}=W_0(T_2R_0)$, and $a_{15}=-Q_0(T_3R_0)$.

In Row 2

From the boundary conditions on H_z at $r = R_0$ we find

$a_{21}=F_1a_{11}$, $a_{22}=F_2a_{12}$, $a_{23}=F_1a_{13}$, $a_{24}=F_2a_{14}$, and $a_{26}=a_{15}$.

In Row 3

From the boundary conditions on E_θ at $r = R_0$ we find

$a_{31}=iL_{12}T_1Q_0'(T_1R_0)$, $a_{32}=iL_{22}T_2Q_0'(T_2R_0)$, $a_{33}=iL_{12}T_1W_0'(T_1R_0)$, $a_{34}=iL_{22}T_2W_0'(T_2R_0)$, and $a_{36}=-kQ_0'(T_3R_0)/T_3$.

In Row 4

From the boundary conditions on H_θ at $r = R_0$ we find

$a_{41}=a_{31}L_{14}/L_{12}$, $a_{42}=a_{32}L_{24}/L_{22}$, $a_{43}=a_{33}L_{14}/L_{12}$, $a_{44}=a_{34}L_{24}/L_{22}$, and $a_{45}=ia_{36}/\eta$.

In Row 5

From the boundary conditions on E_z at $r = R_w$ we find

$a_{51}=Q_0(T_1R_w)$, $a_{52}=Q_0(T_2R_w)$, $a_{53}=W_0(T_1R_w)$, and $a_{54}=W_0(T_2R_w)$.

In Row 6

From the boundary conditions on E_θ at $r = R_w$ we find

$a_{61}=L_{12}T_1Q_0'(T_1R_w)$, $a_{62}=L_{22}T_2Q_0'(T_2R_w)$, $a_{63}=L_{12}W_0'(T_1R_w)$, and $a_{64}=L_{22}T_2W_0'(T_2R_w)$.

APPENDIX C

In the main body of the text Q_0 represents an unmodified or a modified Bessel function of the first kind, W_0 represents an unmodified or a modified Bessel function of the second kind. Q_0' or W_0' represents the derivative of the function with respect to its argument.

Any of the standard texts on Bessel functions give the following formulas:[26,27]

Let $Z_n(X)$ be an unmodified Bessel function of either the first or the second kind of order n.

Then $Z_0'(X) = - Z_1(X)$

and $Z_1'(X) = Z_0(X) - Z_1(X)/X.$

For modified Bessel Functions

of the first kind

$$I_0'(X) = I_1(X)$$

and $I_1'(X) = I_0(X) - I_1(X)/X.$

For modified Bessel Functions

of the second kind

$$K_0'(X) = K_1(X)$$

and $K_1'(X) = - K_0(X) - K_1(X)/X.$

The necessary integral formulas are

for the unmodified Bessel function of the first kind

$$\int_0^r rJ_1^2(X)dr = (1/2)r^2[J_1^2(X) + J_0^2(X) - 2J_0(X)J_1(X)/X],$$

and for the modified Bessel function of the first kind

$$\int_0^r rI_1^2(X)dr = -(1/2)r^2[I_0^2(X) - I_1^2(X) - 2I_0(X)I_1(X)/X].$$

REFERENCES

1. A. J. Lichtenberg, Plasma Waveguides As High Q Structures, University of California Electronics Research Laboratory, Report No. 247, Sept. 1959.
2. G. August, Plasma Confinement of Electromagnetic Waves, University of California Electronics Research Laboratory, Report No. 398, Aug. 1961.
3. Professor J. R. Woodyard (University of California, Berkeley), private communication, 1965.
4. G. August, Coulomb Collisions in Strong Electric Fields, University of California Electronics Resarch Laboratory, Report No. 397, Aug. 1961.
5. A. J. Lichtenberg, P. Govindan, and J. R. Woodyard, Microwave Loss in a Reflex Plasma Discharge, J. Appl. Phys. 38 [1], 382-389 (1967).
6. I. P. Shkarofsky, Values of the Transport Coefficients in a Plasma for Any Degree of Ionization Based on a Maxwellian Distribution, Can. J. Phys. 39, 1619 (1961).
7. L. Spitzer, Physics of Fully Ionized Gases (Interscience Tracts on Physics and Astronomy, New York, 1956).
8. A. W. Trivelpiece, Slow Wave Propagation in Plasma Waveguides, California Institute of Technology Electron Tube and Microwave Laboratory, Tech. Report No. 7, May 1958.
9. H. Gamo, The Faraday Rotation of Waves in Circular Waveguide, J. Phys. Soc. of Japan, 8, 176(1953).

10. W. P. Allis, S. J. Buchsbaum, and A. Bers, Waves in Anistropic Plasmas (M.I.T. Press, Cambridge, 1963), Chapt. 9.

11. V. Bevc and T. E. Everhart, Fast-Wave Propagation in Plasma-Filled Waveguides, J. Electronics Control 13, 185 (1962).

12. J. L. Shohet, Exact Solutions for the Eigenfrequencies of a Microwave Cavity Partially Filled with a Magnetized Plasma, Princeton University Plasma Physics Laboratory, Princeton, N.J., MATT-390, Feb. 1966.

13. M. Goldstein, M. Kresge, and S. Chen, Bessel Functions for Complex Argument and Order, New York University, July 1960 (FORTRAN IV)

14. R. L. Pexton, and D. L. Wilbur, Bessel Function, $K_n(X)$, Lawrence Radiation Laboratory, Berkeley, California, C3-BKY-BESNKS, Aug. 1965 (FORTRAN IV).

15. C. Rugge, Logarithm of the Gamma Function for Complex Arguments, Lawrence Radiation Laboratory, Berkeley, California, C3-BKY-LNGM, Nov. 1964 (FORTRAN IV).

16. National Bureau of Standards, Tables of Bessel Function $J_0(Z)$ and $J_1(Z)$ for Complex Arguments (Columbia University Press, New York, 1950).

17. National Bureau of Standards, Tables of Bessel Function $Y_0(Z)$ and $Y_1(Z)$ for Complex Arguments (Columbia University Press, New York, 1950).

18. J. E. Katz, Complex Determinant Evaluator, Lawrence Radiation Laboratory, Berkeley, California, F3-BKY-CDET, Mar. 1965 (FORTRAN IV).

19. R. V. Churchill, Complex Variables and Applications (McGraw-Hill Book Company, New York, 1960).

20. F. B. Hildebrand, Introduction to Numerical Analysis (McGraw-Hill Book Company, New York, 1956).

21. R. W. Hamming, Numerical Methods for Scientists and Engineers (McGraw-Hill Book Company, New York, 1962).

22. L. Meissner, et al, Matrix Inversion and Linear Systems, Well-Conditioned, Complex, Lawrence Radiation Laboratory, Berkeley, California, F1-BKY-CMXDIV, Aug. 1966 (FORTRAN IV).

23. J. A. Stratton, Electromagnetic Theory (McGraw-Hill Book Company, New York, 1941).

24. S. Ramo, and J. R. Whinnery, Fields and Waves in Modern Radio John Wiley and Sons, Inc. New York, 1953).

25. L. Vardas, Romberg Integration, Lawrence Radiation Laboratory, Berkeley, California, D1-BKY-RMBRG, Sept. 1966 (FORTRAN IV).

26. G. N. Watson, Theory of Bessel Functions (Cambridge University Press, London, 1922).

27. N. W. McLachlan, Bessel Functions for Engineers (Oxford University Press, London, 1962).